The Chemistry of Rhodium and Molybdenum Isocyanide Complexes

Thesis by
Nathan Saul Lewis

In Partial Fulfillment of the Requirements
for the Degree of
Master of Science

California Institute of Technology
Pasadena, California
1977

(Submitted May 31, 1977)

ACKNOWLEDGMENT

I would like to thank my family away from home, the entire Gray group, for making life at Caltech enjoyable and chemistry just plain fun. I would like to extend a special thanks to Penney Slusser, Kim Tyler, and Yo, who have always been there whenever I wanted to talk to them. I thank Bill Trogler and Dave Tyler for being good friends as well as for their invaluable help as chemists. I owe an unpayable debt of gratitude to Kent Mann, who asked a shy freshman four years ago if he would like to come and work for about three hours a week in Harry Gray's lab. Through all these four years, Kent has been understanding, helpful, and unbelievably tolerant of my stupid questions and rotten experiments. In addition to teaching me all I know about experimental chemistry, he has also taught me to think logically and to ask basic questions about an experiment before rushing off to perform it. To Harry Gray, all I can say is that there is no man I respect more, or whose respect I value more highly. In addition to being a good advisor, you're unbeatable at tennis, volleyball, ping-pong, and most importantly, as a human being. Finally, I would like to thank my parents, who have put up with me every weekend, and their untiring advice has made it easy for me to do well in my studies and in the lab.

ABSTRACT

The rhodium isocyanide dimer, $Rh_2(bridge)_4^{2+}$, has been synthesized and characterized. Like monomeric rhodium isocyanide complexes, the dimer has a tendency to associate in solution and reversibly form oligomers. These oligomers have been detected spectroscopically, and concentration dependences verify their formulation as high aggregates. The dimer also undergoes two-center, two-electron oxidative addition with a variety of reagents, including the halogens, methyl iodide, ethyl iodide, and methyl tosylate. These oxidative adducts have been characterized and studied through a variety of techniques. The dimer, unlike rhodium isocyanide monomers, acts as a base and binds one proton in aqueous solution. Titration data are presented, and an approximate pK_b has been obtained. When treated with aqueous acid, visible light (546 nm) photolysis of solutions of $Rh_2(bridge)_4^{2+}$ yields molecular hydrogen with quantum yields as high as 0.04. The photochemistry is oxygen sensitive, as well as anion dependent. Possible means of exploiting the photoreaction in a solar energy storage scheme is also discussed. In order to better understand the metal-metal interactions in the dimeric species, extended-Huckel molecular orbital calculations were performed on the rhodium dimer, as well as on monomeric fragments with the four isoelectronic metals Ru(0), Pd(II), Co(I), and Ir(I). These results, and their relationship to observed physical properties of the rhodium dimer are discussed in detail.

TABLE OF CONTENTS

CHAPTER 1

A STUDY OF THE CHEMISTRY OF THE DIMERIC RHODIUM ISOCYANIDE COMPLEX; $Rh_2(bridge)_4^{2+}$

Introduction

There has been much interest in the development and characterization of materials which exhibit anisotropic properties in the solid state.[1-8] These compounds, often termed "one dimensional materials", display huge variations in physical properties depending upon the particular orientation of the material to be tested. Perhaps the most widely studied examples of such transition metal complexes involve long chains of platinum(II), and include $(Pt(NH_3)_4)(PtCl_4)$ (Magnus' Green Salt)[1] and $K_2Pt(CN)_4Cl_{0.3}$ (Krogmann's Salt).[2] These compounds exhibit very high anisotropic effects and show unusual conductivity properties along the unique molecular axis. The major drawback with the Pt(II) compounds is that study of these complexes is restricted to a determination of solid state properties because these compounds have a strong tendency to disproportionate in solution and lose their anisotropy.

In order to obtain anisotropic materials more suitable for solution characterization, a study of rhodium(I) isocyanide complexes was undertaken in 1974 by Harry Gray and Kent Mann at Caltech.[9,10] The rhodium system was seen to have two significant improvements over the platinum complexes: 1) the choice of rhodium instead of platinum as the coordination center would lead to more tractable complexes, and 2) the wide variety of side groups present in the isocyanide ligands permitted detailed comparisons of many different ligands, and thus enabled one to identify major steric and electronic factors which might play a role in the solid state properties.

These rhodium complexes were indeed found to exhibit solid-state

properties similar to the Pt(II) complexes; however, the rhodium(I) isocyanide complexes were also found to possess many of these properties in solution as well. Detailed spectral studies as a function of concentration indicated that the $Rh(CNR)_4^+$ cations undergo complicated equilibria in solution, and this data was interpreted as the formation of oligomers of the type $(Rh(CNR)_4^+)_n$ which are in equilibrium with the parent monomers. Though the observations and data were logically consistent with the formation of these oligomers, the complicated equilibria involved prevented isolation of these species.[11] In order to provide direct evidence for the formation of the postulated dimers and higher order oligomers, it was proposed by Kent Mann that a bridging isocyanide ligand that would "lock together" two rhodium(I) units should be synthesized. The main focus of the first portion of this work deals with the synthesis and characterization of such a discrete rhodium(I) isocyanide dimer, $Rh_2(CN(CH_2)_3NC)_4^{2+}$, or $Rh_2(bridge)_4^{2+}$, and the relation of this dimeric species to its equilibria-formed counterparts.

After a preliminary examination of the properties and characteristics of the new dimer, it was realized that the high degree of electronic coupling between the two rhodium centers might lead to unique redox properties for this system. The remainder of the work, in a general sense, deals with the unusual reactivity due to this strong coupling between the rhodium centers induced by the bridging ligand framework. This chemistry encompasses two center oxidative addition reactions, reversible protonations of the dimer, and energy storing photochemical systems. Though monomeric complexes may exhibit properties similar to those found for the bridged dimer, I feel that the basic theme of this thesis is the unique properties of two strongly coupled

d^8 metal systems, and emphasize that the reader should be always cognizant of these properties in the chemistry to be presented.

Experimental Techniques

Spectral Measurements

Infrared spectra were recorded on a Perkin-Elmer 225 spectrophotometer as Nujol mulls or KBr pellets, as indicated in the text. Nuclear magnetic resonance experiments were performed on Varian T-60 and A-60 spectrometers, except when experiments required Fourier transform techniques, and a Varian XL-100 spectrometer was used in these instances. Electronic absorption spectra were measured using a Cary 17 spectrophotometer. Emission spectra were obtained using a Perkin-Elmer MPF-3A flourescence spectrometer and spectra were digitally corrected for phototube and monochrometer response before data analysis was undertaken.[9] All pH measurements were taken on a Brinkman pH-101 meter which was calibrated with known buffer solutions before each experiment. Electron Paramagnetic Resonance experiments were performed on a Varian E-9 spectrometer, and fast kinetics were recorded on a Tektronix Rapid Scanning Spectrometer interfaced with a PDP-11 computer for data storage and analysis.

Photochemical Apparatus

Preparative scale photochemistry was performed by irradiation with 150-watt tungsten light bulbs with Corning 3-68 glass filters. These same filters were also used in conjunction with a 200-watt Hg-Xe Oriel source for use in small sample photolyses. Quantum yields were measured using a 450-watt medium pressure Hanovia mercury lamp equipped with a 546 nm isolation filter. All actinometry was done using $KCr(NH_3)_2(NCS)_4$ (Reinecke's salt) actinometers,[12] with all irradiations carried out in a block thermostatted with

approximately 30 liters of distilled water.

Synthetic Techniques

All solvents used for synthesis were obtained from commercial sources as reagent grade or better, and were used without further purification. Except for the photochemistry, all compounds are air stable and thus did not necessitate vacuum line techniques. Photochemical experiments were rigorously degassed by at least three freeze-pump-thaw cycles under an oil diffusion pump. Analytical data was supplied by either the Caltech Microanalytical Lab, Pasadena, CA., Chemalytics, Tempe, Arizona, or Galbraith Laboratories, Knoxville, Tennessee. All samples for analysis were dried overnight and pumped on at less than 10^{-6} mm Hg for at least 12 hours before submission for analysis.

Preparation of Materials

1-3-diisocyanopropane (bridge)

This previously unreported compound was synthesized by the general method of Ugi, et. al,[13] but several minor modifications critical to isolation of the product warrant a complete description of the method used.

To a 3 liter, 3-necked flask equipped with overhead stirrer and two Claisen condensors was added 600 ml of a 50% aqueous solution of NaOH (prepared by mixing excess solid NaOH and water and allowing the phases to come to equilibrium at 25 °C. over several days) and 170 ml (2.1 moles) of chloroform . 500 ml of dichloromethane was added as solvent, followed by 84 ml (1 mole) of 1-3-diaminopropane (Aldrich Chemical Company) and finally, 2.1 g of the phase-transfer catalyst, benzyl-triethylammonium chloride. The mixture was then rapidly stirred until refluxing of the dichloromethane was observed. When the rate of reflux becomes excessive, the stirring rate is decreased to slow the reaction; caution is advised, as pressure explosions of solvent gushing out the condensors may occur if the reaction rate is too rapid. The flask temperature should be maintained at about 40°C. for 30 minutes, after which the stirring may be accelerated once again. The reaction mixture is stirred for about three additional hours, and the solution will have darkened slightly due to formation of polymeric side product. The layers are separated, and the organic phase is washed four times with 500 ml portions of water. The solvent is then removed, and the ligand is purified by vacuum distillation. The bridge distills at 55 °C. at 1mm Hg as a clear liquid. Use Caution: two violent explosions have occurred during

distillation; in both instances, the solutions had an orange color just before exploding, however, this correlation may just be coincidental. In any case, use extreme care while distilling the product. The infrared spectrum of the ligand shows a very strong and narrow ν (C≡N) stretch at 2140 cm^{-1}, with other prominent peaks at 2930 (m), 1660 (m), and 1490 (s) cm^{-1}. The 60 MHz PMR spectrum of bridge exhibits two multiplets integrated in the ratio of 2:1, the first is a triplet of triplets at 3.48 δ (terminal CH_2), and the second is a complex multiplet centered at 1.76 δ (central CH_2). With small amounts of the material, an alternative, safer purification is elution of crude product with toluene over alumina, with pure bridge being the first fraction off the column.

1-3-diformamidopropane

In order to develop a safer method of preparing bridge, the corresponding formamide was prepared, to be dehydrated and yield the isocyanide. To 84 ml (1 mole) of 1-3-diaminopropane was added dropwise 163 ml (2.2 moles) of ethyl formate, and the mixture was stirred for two hours. The ethanol formed was removed by rotary evaporation, yielding pure 1-3diformamidopropane. The product exhibits a 60 MHz PMR spectrum consisting of a sharp singlet at 8.10 δ, broad singlet at 7.80 δ, quartet at 3.15 δ, and a quintet at 1.82 δ, integrating in the ratios 1:1:2:1 respectively. Attempts to dehydrate the formamide via conventional methods such as the $POCl_3$/pyridine;[14] $POCl_3$/Triethyl amine/CH_2Cl_2,[15-17] $POCl_3$/quinoline,[18] para-tolunesulfonyl chloride/pyridine all failed; however, it is very likely that the dehydration method employing the PPh_3/CH_2Cl_2/Triethyl amine[19,20] system will work, as it was successful in dehydrating the very unstable

2-formamidopyridine (see section 2).

1-4-diisocyanobutane

Method was the same as described for bridge, but used the 1-4 diaminobutane as starting amine. The product boils at 65 °C. at 1.3 mm Hg as a clear liquid whose 60 MHz PMR shows broad multiplets at 3.42 δ and 1.86 δ in the ratio of 2:1.

$(Rh(1\text{-}5\text{-cyclooctadiene})Cl)_2$

This compound was synthesized without modification by the method of Chatt et al.[21]

$Rh_2(bridge)_4(BF_4)_2$

To a solution of 1.23 g of $(Rh(COD)Cl)_2$ in 20 ml of acetonitrile was added 0.97 g of silver tetrafluoroborate in 10 ml of acetonitrile. The solution was stirred and filtered by gravity to remove the silver chloride formed. Then 0.94 g of bridge in 10 ml of acetonitrile was added dropwise with stirring to the rhodium solution. The purple powder was filtered, washed with diethyl ether, and dried in vacuo.[22] This salt is soluble in acetonitrile, DMF, and DMSO. Calc: C 31.78, H 3.20, N 14.82, F 20.11 Found: C 31.62, H 3.37, N 14.66, F 19.82.

$Rh_2(bridge)_4Cl_2$

This compound was obtained by adding a stoichiometric amount of bridge to a chloroform solution of $(Rh(COD)Cl)_2$ and filtering the blue precipitate, washing with diethyl ether, and drying in vacuo. Soluble in methanol, water, DMSO, and DMF.[23]

$Rh_2(bridge)_4(BPh_4)_2 \cdot 2CH_3CN$

A stoichiometric amount of $NaBPh_4$ in methanol was added to a methanol solution of $Rh_2(bridge)_4Cl_2$. The purple solid was recrystallized from acetonitrile. Calc: C 66.37, H 5.41, N 10.75 Found: C 65.59, H 5.49, N 10.24 . ν(C≡N) at 2172 cm^{-1} as a KBr pellet. 60 MHz PMR: broad multiplets at 3.78 δ and 1.98 δ in a 2:1 ratio in d^6 DMSO (peak due to acetonitrile was also observed. Soluble in acetonitrile, DMSO, acrylonitrile.

Other salts made included $Rh_2(bridge)_4X_2$ where X= NO_3, PF_6, Br, I, ClO_4, Tosylate, but none of these were more tractable than the ones above.

$(Rh_2(bridge)_4I_2)(I_3)_2$

This complex was prepared by addition of I_2 to a warm acetonitrile solution of $Rh_2(bridge)_4(BPh_4)_2$. The product was isolated as red crystals on cooling. Calc: C 15.04, H 1.50, N 7.05, I 63.55 Found: C 15.82, H 1.65, N 7.09, I 62.22 ν(C=N) 2227 cm^{-1} as KBr pellet. No EPR spectrum was observed.

$(Rh_2(bridge)_4Br_2)(Br_3)_2$

Synthesis was as for I_2 adduct above, and cooling the solution gave yellow crystals. Calc: C 19.67, H 1.98, N 9.17 Found: C 19.97, H 1.93, N 9.06 ν(C≡N) 2230 cm^{-1} as a KBr pellet.

$(Rh_2(bridge)_4Br_2)Br_2 \cdot 2H_2O$

A solution of $Rh_2(bridge)_4Cl_2$ in concentrated aqueous HBr was photolyzed ($\lambda \geq 520$ nm). Yellow crystals were isolated from the solution

after ten hours of photolysis with a 150 watt tungsten light bulb. The spectral properties are identical with the $(Rh_2(bridge)_4Br_2)(Br_3)_2$ sample prepared thermally as above. Calc: C 25.61, H 3.01, N 11.95, Br 34.08 Found: C 25.71, H 3.04, N 11.90, Br 34.00

$(Rh_2(bridge)_4(CH_3)(I))(BPh_4)_2 \cdot 2CH_3CN$

A stoichiometric amount of CH_3I was added to a solution of $Rh_2(bridge)_4(BPh_4)_2 \cdot 2CH_3CN$ in acetonitrile. Upon slow addition of diethyl ether, reddish brown crystals were obtained, filtered, washed with diethyl ether, and dried in vacuo. Calc: C 60.66, H 5.09, N 9.69 Found: C 58.74, H 5.08, N 9.29 $\nu(C\equiv N)$ at 2183 and 2212 cm^{-1} as a KBr pellet. The 60 MHz PMR exhibits broad multiplets at 4.08 δ (terminal CH_2), 2.18 δ (central CH_2) and a doublet at 1.38 δ (CH_3 coupled to spin $\frac{1}{2}$ ^{103}Rh nucleus). Peaks were also observed for the acetonitrile and tetraphenylborate protons. Integration of the resonances verified the structure as formulated.

References

1. D. S. Martin, Jr., R. M. Rush, R. F. Kroening, and P. E. Fanwick, Inorg. Chem., 12, 301 (1973).
2. K. Krogmann, Angew. Chem. Internat. Ed., 8, 35 (1969).
3. H. R. Zeller, Adv. Solid State Physics, 13, 31 (1973).
4. H. Isci and W. R. Mason, Inorg. Chem., 13, 1175 (1974).
5. P. Day, A. F. Orchard, A. J. Thompson, and R. J. P. Williams, J. Chem. Phys., 42, 1973 (1965).
6. B. G. Anex, M. E. Ross, and M. W. Hedgecock, J. Chem. Phys., 46, 1090 (1967).
7. B. D. Silverman, B. A. Scott, J. Chem. Phys., 63, 518 (1975).
8. B. D. Silverman, B. A. Scott, J. Chem. Phys., 63, 523 (1975).
9. Kent Mann, Ph. D. Thesis, California Institute of Technology, 1976.
10. K. R. Mann, J. G. Gordon, II, and H. B. Gray, J. Amer. Chem. Soc., 97, 3553 (1975).
11. A subsequent crystal structure of $Rh(CNPh)_4(BPh_4)$ indicates that it crystallizes as discrete dimers in the unit cell; see K. R. Mann, N. S. Lewis, R. M. Williams, J. G. Gordon, II, and H. B. Gray, J. Amer. Chem. Soc., to be submitted for publication.
12. E. E. Wegner and A. W. Adamson, J. Amer. Chem. Soc., 88, 394 (1966).
13. W. P. Weber, G. W. Gokel, and I. K. Ugi, Angew Chem. Internat. Edit., 11, 530 (1972).
14. J. Casanova, Jr., R. E. Schuster, and N. D. Werner, J. Org. Chem., 31, 3473 (1966).
15. F. Lautenschlager and G. F. Wright, Can. J. Chem., 41, 863 (1963).
16. K. Pilgram and F. Korte, Tetrahedron Lett., 881 (1966).

17. I. Ugi and R. Meyr, Angew. Chem., 70, 702 (1958).

18. I. Ugi, R. Meyr, M. Lipinski, F. Bodesheim, and F. K. Rosendahl, Org. Syn., 41, 13 (1961).

19. U. Schollkopf, F. Gerhart, I. Hoppe, Justis Liebes Ann. der Chemie., 1, 183 (1976).

20. R. Appel, R. Kleinstuck, and K. D. Ziehn, Angew. Chem. Internat. Ed., 10, 132 (1971).

21. J. Chatt and L. M. Venanzi, J. Chem. Soc. (A), 4735 (1957).

22. The filtrate from this preparation was a deep blue, with two bands in the electronic absorption spectrum at 580 and 310 nm. This species probably represents polymeric metal chains or partially chelated metal centers.

23. The infrared spectrum was unavailable because this particular salt does not grind to a powder, but mashes instead, and this makes it impossible to prepare KBr pellets or Nujol mulls of the salt. Its electronic absorption spectrum matches that of the BF_4^- and BPh_4^- salts.

Results and Discussion

Electronic Properties and Oligomerization Reactions

The rhodium (I) isocyanide monomers have been known for some time, and their chemistry has been studied by several investigators.[1,2] One of the most interesting characteristics of these compounds is their tendency to associate in solution and form long chains of monomers stacked in a face-to-face fashion. These reactions have been studied by Mann and Gray; however, the oligomers detected spectroscopically were never directly isolated from solution.[3,4] The purpose of synthesizing a rhodium (I) isocyanide dimer was to model the properties of the oligomers previously observed, and to relate the properties of this discrete dimer to the dimeric species formed by monomeric association equilibria.

To this end, the ligand 1-3-diisocyanopropane was synthesized, as the three methylene bridge would be long enough to easily bind two rhodium atoms, yet short enough to avoid chelation to one metal center. When the ligand is added to solutions of (Rh(1-5-cyclooctadiene) $(CH_3CN)_2$ $(BF_4)_2$ in acetonitrile, a deep blue solid of the rhodium dimer, $Rh_2(bridge)_4(BF_4)_2$ is obtained. As steric considerations rule out bidentate coordination for the bridge ligand at a single rhodium center, we assume that the structure of $Rh_2(bridge)_4^{2+}$ is as shown in figure 1 .

The electronic absorption spectrum of this dimer shows a striking similarity to the equilibria-formed dimeric species previously studied, with intense bands at 318, 343, and 555 nm in methanol solution. In order to understand the similarities of $Rh_2(bridge)_4^{2+}$ to the other monomeric and dimeric species, we must appeal to molecular orbital theory. A simplified energy level diagram for a monomeric d^8 $Rh(CNR)_4^+$ complex has been formulated previously,[5] and possesses

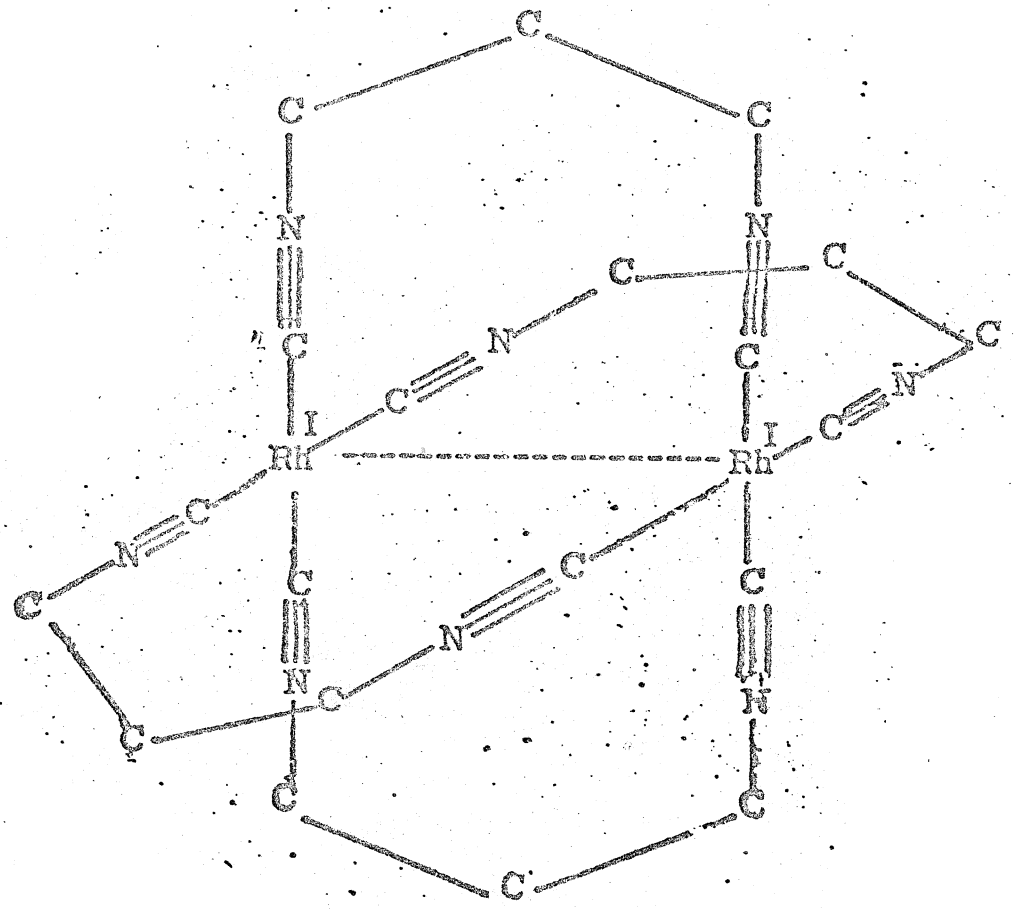

Figure 1

Structure of $Rh_2(bridge)_4^{2+}$

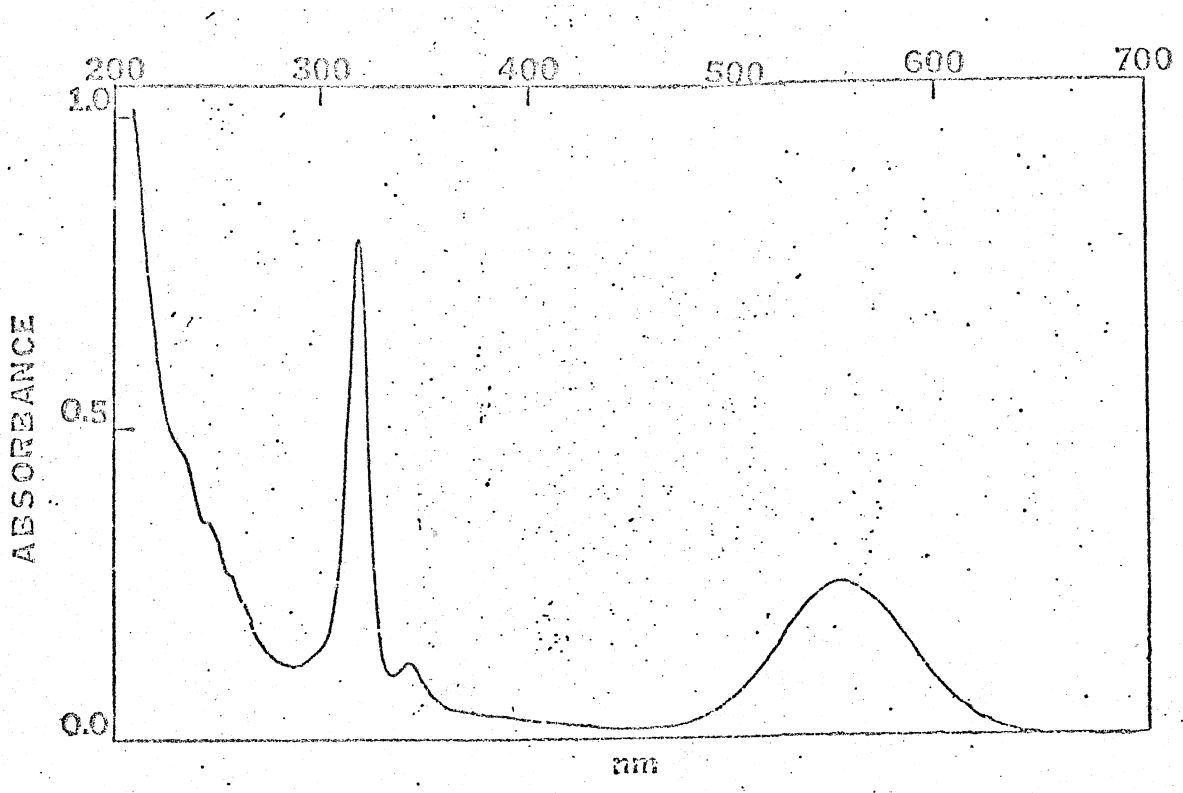

Figure 2
Electronic absorption spectrum of $Rh_2(bridge)_4Cl_2$ in methanol solution.

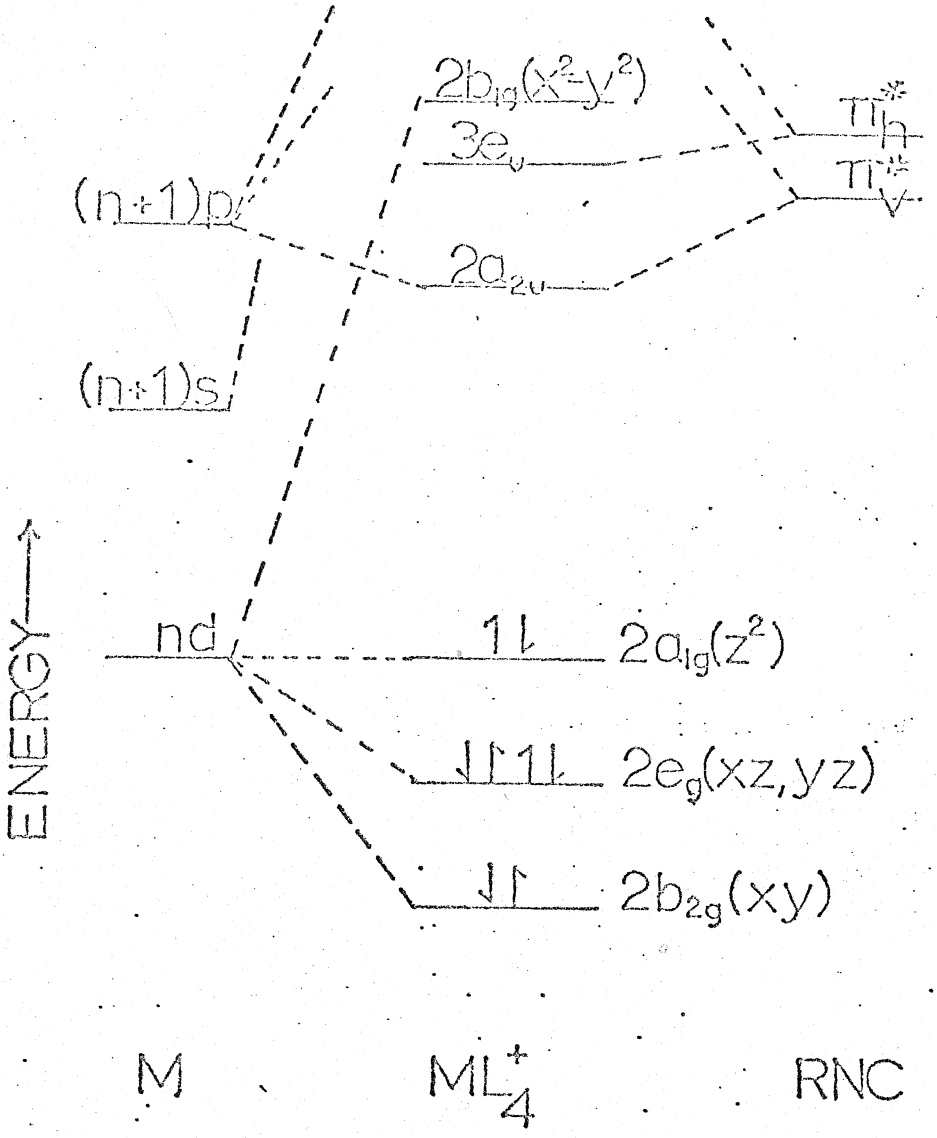

Figure 3

MO Energy Diagram for $M(CNR)_4^+$

the orbital energy ordering of $b_{2g}(xy) < e_g(xz, yz) < a_{1g}(dz^2) < a_{2u}(\pi^*) < b_{1g}(x^2-y^2)$. As we bring two monomers together to form a dimeric unit, either through equilibria or by use of bidentate ligands, the orbitals which interact the most are the $a_{1g}(dz^2)$ and the $a_{2u}(\pi^*)$ orbitals. Both these orbitals are perpendicular to the molecular plane, and therefore will have high overlap as the Rh-Rh distance decreases. Forming molecular orbitals for the dimer involves taking symmetric and antisymmetric combinations of each of these orbitals, leading to bonding and antibonding combinations, as shown in figure 4 with the proper D_{4h} symmetry labels. As both components of the monomeric a_{1g} (dz^2) orbital are fully occupied in the dimer, there is no direct gain in stability due to this splitting. However, the a_{2u} LUMO in the monomeric species also splits into a_{1g} and a_{2u} components, and interaction of these orbitals with the $1a_{1g}$ and $1a_{2u}$ orbitals stabilizes the latter, resulting in a bonding situation for the dimer. These bonding interactions must be fairly substantial, as they are able to overcome the unfavorable coulombic forces between cationic units as well as the repulsive Pauli exclusion pair-pair effects of bringing together two fully occupied orbitals.

As the pair-pair repulsions mentioned above might be fairly substantial, an argument may be advanced that the above MO formulation is incorrect, and that in actuality, the splitting between the two lowest levels is so great that the $2a_{1g}$ orbital is actually lower in energy than the $1a_{2u}$ level, resulting in a configuration in which all four electrons are in "bonding" orbitals, $(1a_{1g})^2 (2a_{1g})^2$. However, this formulation predicts that as the bond length is increased, the repulsive interactions should be minimized and the lowest transition should red shift. This is

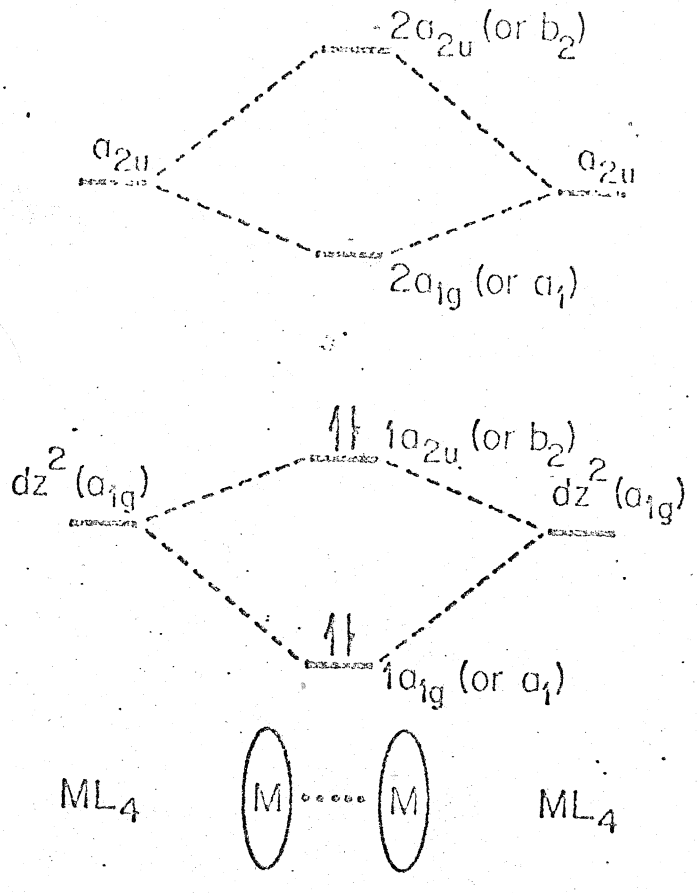

Figure 4

MO Diagram for $(M(CNR)_4^+)_2$

in contrast to the first formulation, which predicts a blue shift of the low energy band upon bond lengthening. As can be seen for the series $Rh(CNR)_4^+$, where R=t-butyl and isopropyl[1], decreasing the steric interactions (presumably leading to shorter Rh-Rh bond lengths) results in a red shift of the lowest energy transition, in contrast to the latter MO formulation. Furthermore, for the rigid dimeric complexes of $Rh_2(bridge)_4^{2+}$ and $Rh_2(CN(CH_2)_4NC)_4^{2+}$, the latter compound containing one additional methylene group in the bridging ligand, the lowest energy transition is found to blue shift as the bond distance is lengthened,[6] again consistent with the first formulation of bonding for the dimers.

The MO analysis above indicates that the $Rh_2(bridge)_4^{2+}$ absorption at 555 nm in methanol may be assigned to the fully allowed $1a_{2u} \rightarrow 2a_{1g}$ transition. As noted previously, this assignment is justified by analogy to the $Rh(CNPh)_4^+$ dimerization, in which a 568 nm band is observed at high Rh(I) concentration, and is assigned to the dimeric species formed by an equilibrium process. The invariance of the 318 and 343 nm transitions from the $Rh(CNAlkyl)_4^+$ monomers[1,3,4] implies that these excitations are due to electrons not involved in metal-metal bonding, and as such can be assigned as the $^1A_{1g} \rightarrow {}^1E_u$ and $^1A_{1g} \rightarrow {}^3E_u$ states respectively. The magnetic circular dichroism spectra of $Rh_2(bridge)_4(BPh_4)_2$ confirm these assignments, showing a B term for the 555 nm band and A terms for the 318 and 343 nm bands. This indicates that the high energy transitions lead to orbitally degenerate excited states, consistent with the ^1E and ^3E assignments, and the presence of the B term at 555 nm reinforces that assignment as a $^1A_{2u}$ state.

Table 1

Band positions for the lowest spin-allowed transitions of oligomers of the type $(Rh(CNR)_4^+)_n$.

Complex	Monomer	Dimer	Solvent
$Rh(CNt\text{-butyl})_4^+$	371	490	H_2O
$Rh(CNi\text{-propyl})_4^+$	383	495	H_2O
$Rh_2(bridge)_4^{2+}$	---	555	CH_3OH
$Rh_2(bridge')_4^{2+}$	---	542	CH_3OH

bridge' = $CN(CH_2)_4NC$

As might be expected from the strong interactions of the dz^2 and π^* orbitals, the energy of the lowest transition is fairly responsive to the distance between metal centers, and this transition energy thus provides a sensitive measure of overlap and bond length. Balch[7] has confirmed this hypothesis, showing that there exists a strong correlation between bond length and the energy of the lowest absorption band in a large variety of rhodium(I) dimers. Since the $Rh(CNPh)_4(BPh_4)$ complex is found to crystallize as discrete dimers in the solid state with a rhodium-rhodium bond length of 3.18 Å, comparison of the band energies of 565nm for $(Rh(CNPh)_4^+)_2$ versus 555 nm for $Rh_2(bridge)_4^{2+}$ leads to a prediction of about 3.2 Å for the rigid dimers.[8] By simple Huckel theory, the energy of the lowest transition is 2β, (where $\beta = \beta_{a_{1g}} + \beta_{a_{2u}}$) yielding a β of approximately 8100 cm^{-1} for $Rh_2(bridge)_4^{2+}$, compared to about 5500 cm^{-1} for equilibrium-type $(Rh(CNAlkyl)_4^+)_2$ dimers. Thus, the higher β for the rigid dimer again reflects the strong coupling present in this system due to the steric constraints of the bridge ligand.

Unlike the monomeric rhodium isocyanide complexes, the $Rh_2(bridge)_4^{2+}$ ion exhibits strong emission in fluid solution at room temperature. Excitation into the lowest energy absorption band of $Rh_2(bridge)_4(BPh_4)_2$ leads to intense luminescence with an undegassed quantum yield of $0.056 \pm .01$. This quantum yield is about 20% greater than that of the highly emissive $Ru(bipy)_3^{2+}$ ion at room temperature in fluid solution.[9,10] The large overlap and small Stokes shift of the emission and absorption bands suggest that the excited state reached in absorption is also the emissive state. As the 555 nm absorption in $Rh_2(bridge)_4^{2+}$ has been assigned to the electric dipole

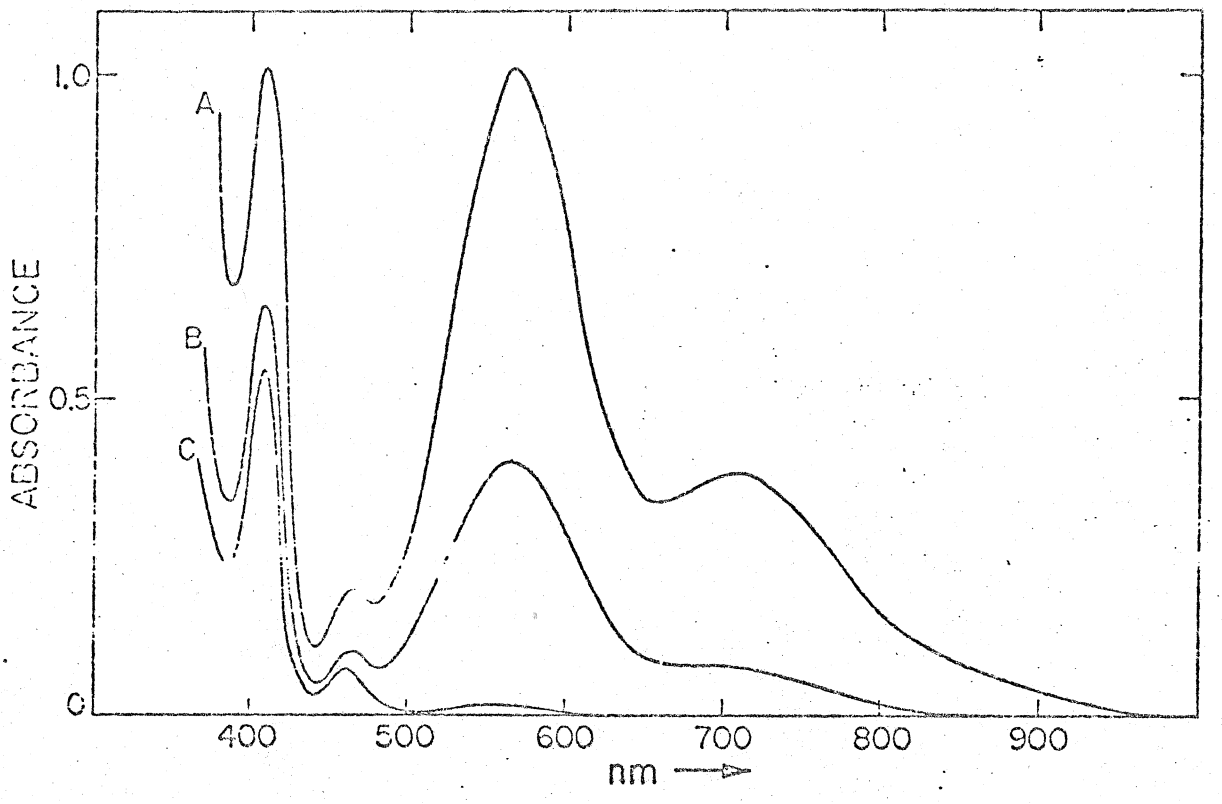

Figure 5

Electronic Absorption Spectrum of $Rh(CNPh)_4(BPh_4)$ in acetonitrile

Note the similarity of the dimer band at 568 to the spectrum of $Rh_2(bridge)_4Cl_2$ in Figure 2.

allowed $^1A_{1g} \rightarrow {}^1A_{2u}$ ($1a_{2u} \rightarrow 2a_{1g}$) transition, the emission at 656 nm is therefore attributed to prompt flourescence which is $^1A_{2u} \rightarrow {}^1A_{1g}$ ($2a_{1g} \rightarrow 1a_{2u}$) in nature. Excitation of $Rh_2(bridge)_4^{2+}$ also gives long-lived transient absorption, which is logically attributed to the triplet state ($^3A_{2u}$) associated with the $1a_{2u} \rightarrow 2a_{1g}$ excitation. A detailed study of the excited state properties of $Rh_2(bridge)_4^{2+}$ and the $(Rh(CNR)_4^+)_2$ dimers has been completed, and contains further information on radiative decay pathways in these systems.[11]

Since the interactions between $Rh_2(bridge)_4^{2+}$ dimers should be comparable to those in the $Rh(CNR)_4^+$ monomers, it is reasonable to expect that $Rh_2(bridge)_4^{2+}$ would also show a tendency to associate in solution. Electronic absorption spectra for three concentrations of $Rh_2(bridge)_4Cl_2$ in methanol[12] are displayed in figure 8. The concentration dependence of the absorption spectrum may be interpreted in terms of the following oligomerization equilibria:

$$D = Rh_2(bridge)_4^{2+}$$

$$2D \overset{K_1}{\rightleftharpoons} D_2 \qquad 3D \overset{K_2}{\rightleftharpoons} D_3 \qquad 4D \overset{K_3}{\rightleftharpoons} D_4 \qquad nD \overset{K_{n-1}}{\rightleftharpoons} D_n$$

As the solution becomes increasingly concentrated, principal low energy bands appear at 778, 990, 1140, and 1735 nm, in addition to the 318, 343, and 555 nm transitions assigned to the dimer itself. Detailed studies of the concentration dependence of these spectra reveal that plots of A_{555} vs $\sqrt{A}_{778}$ and A_{555} versus $\sqrt[3]{A}_{990}$ are straight lines, indicating that the bands at 778 and 990 nm may be assigned to tetrameric and hexameric Rh(I) species. The bands at 1140 and 1735 nm are present only in the most concentrated solutions, and are logically attributable to higher oligomers ($n > 3$). The observed spectroscopic

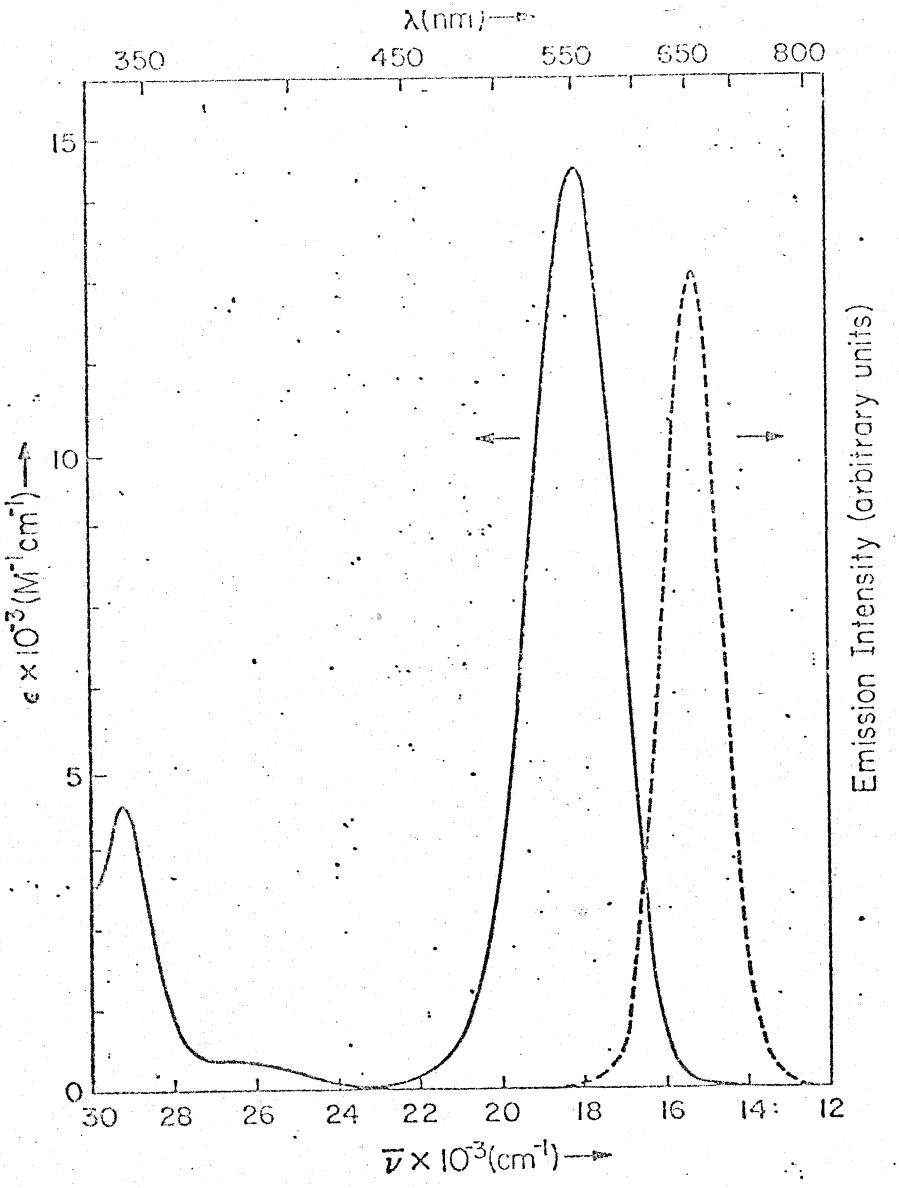

Figure 6
Absorption and emission spectra of
$Rh_2(bridge)_4(BPh_4)_2$ in CH_3CN.

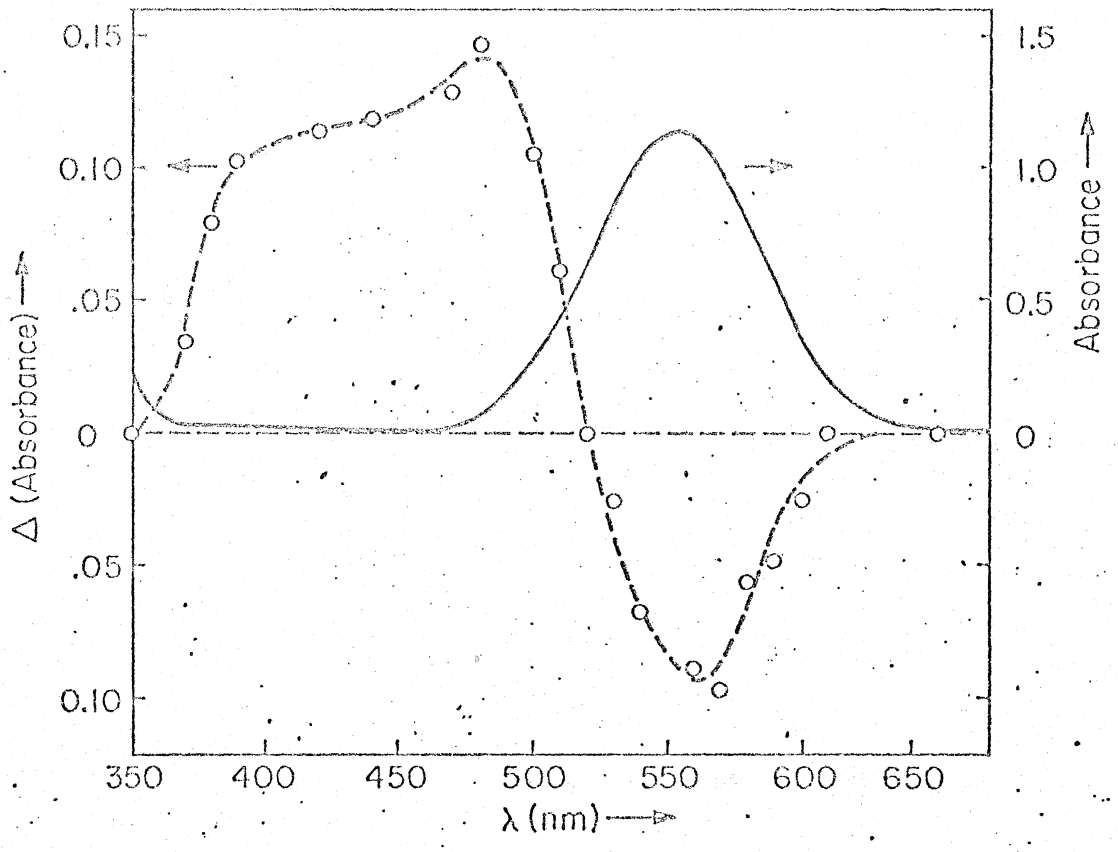

Figure 7

Difference spectrum showing long-lived transient arising from excitation into the 555 nm band of $Rh_2(bridge)_4(BPh_4)_2$. Figure reproduced from reference 11.

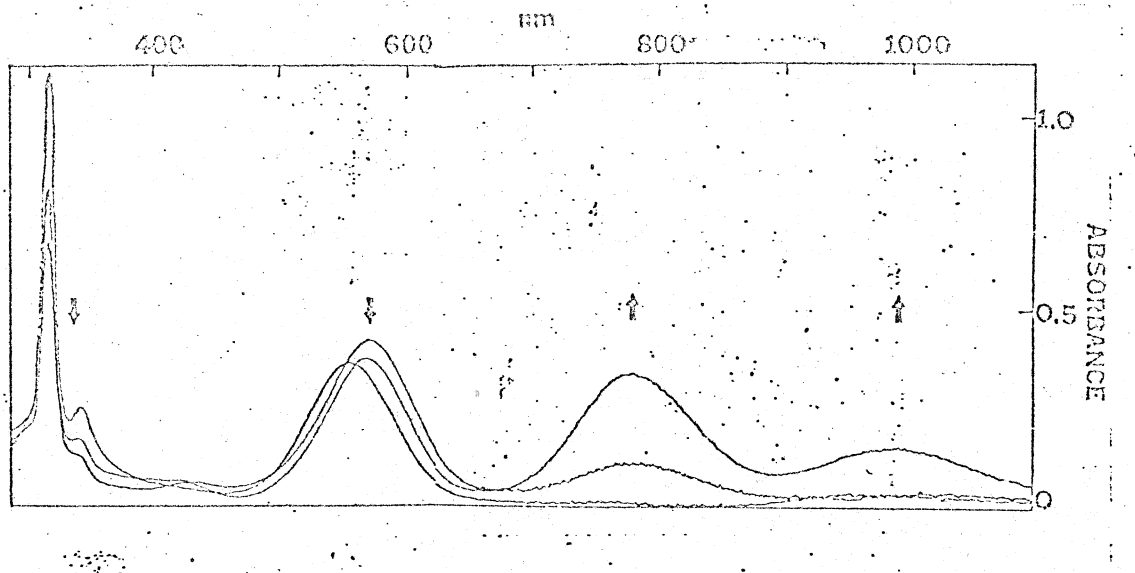

Figure 8

Electronic absorption spectra of $Rh_2(bridge)_4Cl_2$ in methanol as a function of Rh concentration.

Table 2

Absorption data at 555, 778, and 990 nm as a function of $Rh_2(bridge)_4Cl_2$ concentration in CH_3OH.

C(g/l)	A_{555}	A_{778}	A_{990}
7.10	35.97	81.75	79.40
2.84	29.24	48.42	38.09
1.30	18.01	15.90	7.01
1.04	14.97	10.29	4.21
0.52	9.82	2.34	0.58
0.13	1.76	0.00	0.00

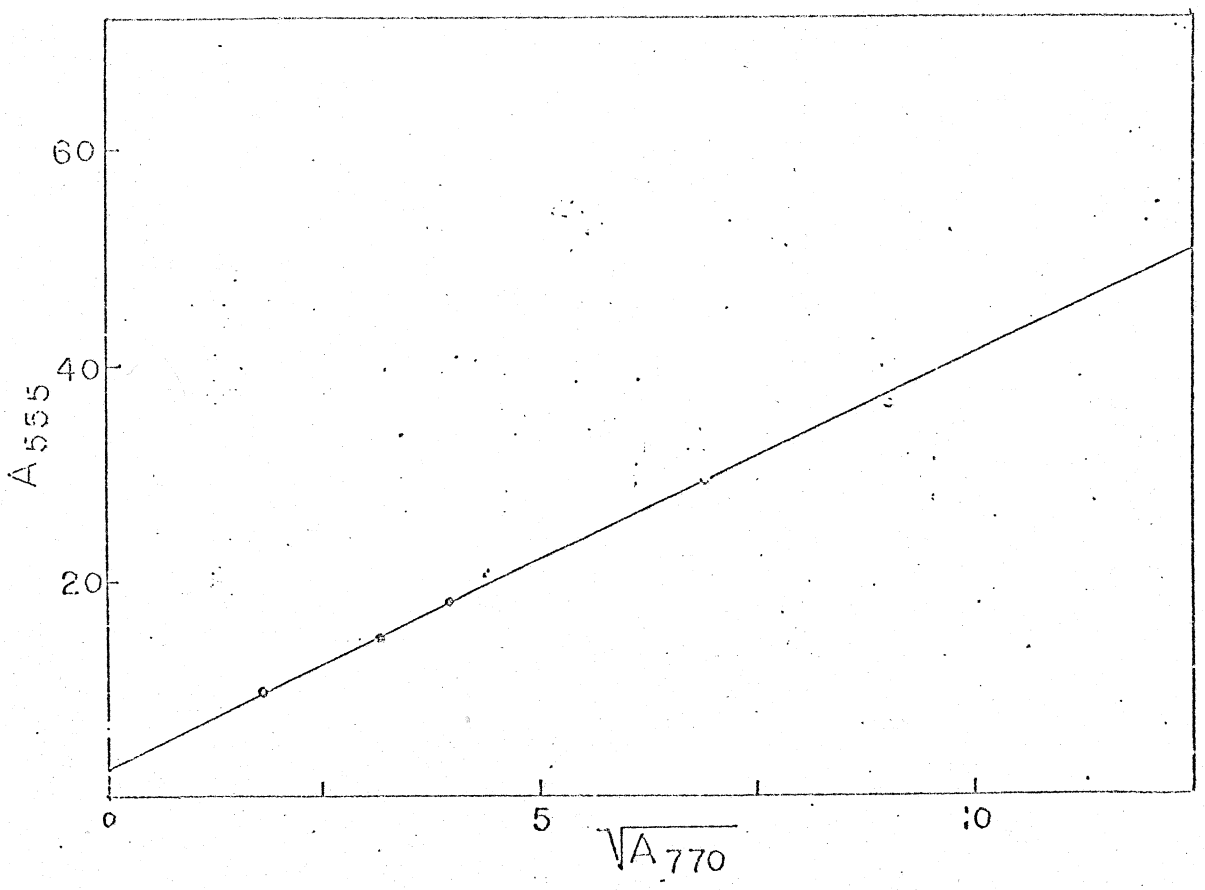

Figure 9
Plot of the square-root of tetramer absorbance vs. dimer absorbance as a function of concentration.

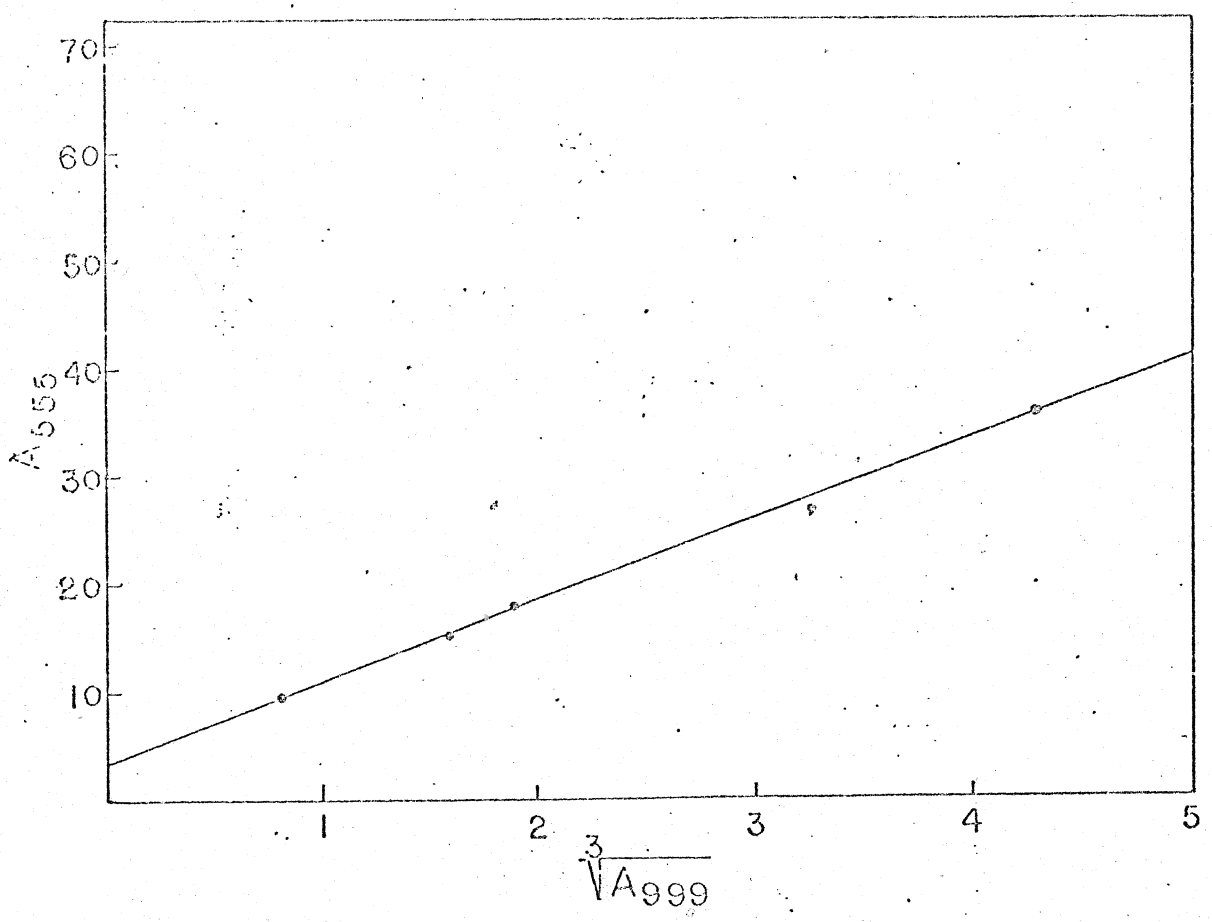

Figure 10

Plot of cube-root of hexamer absorption vs. the dimer absorption as a function of concentration.

behavior of the $Rh_2(bridge)_4^{2+}$ oligomers accords with the simple MO theory previously presented. Analysis of the tetrameric Rh(I) units similar to that carried out for $Rh_2(bridge)_4^{2+}$ itself suggests that the 778 nm band be assigned to the $2a_{2u} \rightarrow 3a_{1g}$ transition, the hexameric Rh(I) absorption at 990 nm is assigned to $3a_{2u} \rightarrow 4a_{1g}$, and the band at 1140 nm may be attributed to $4a_{2u} \rightarrow 5a_{1g}$ in an octameric species.

With a reasonable choice of extinction coefficients for the tetrameric and hexameric rhodium(I) oligomers, approximate values of the equilibrium constants for association may be obtained. The equilibria as defined above and a mass balance on rhodium yield[4] that the slope of A_D vs $\sqrt{A_{D_2}}$ equals $\frac{\epsilon_D}{\sqrt{K_1}\,\epsilon_{D_2}}$, and the slope of A_D vs $\sqrt[3]{A_{D_3}}$ equals $\frac{\epsilon_D}{\sqrt[3]{K_1 K_2}\,\epsilon_{D_3}}$. Using the ϵ_D of 14,500 obtained for ϵ_{555} in dilute solutions of $Rh_2(bridge)_4(BPh_4)_2$ in acetonitrile, as well as values of ϵ_{D_2} (29,000) and ϵ_{D_3} (43,500), allows the calculation of K_1 and K_2. These values for the extinction coefficients of the higher oligomers are justified by several previous studies, in which it has been empirically established that the extinction coefficient of oligomers is roughly proportional to the degree of association.[1-3] The approximate values calculated for the equilibrium constants are $K_1 = 524\ M^{-1}$ and $K_2 = 265\ M^{-1}$, which are found to be similar to those for the monomeric associations.

Simple Huckel theory predictions for the energies of the oligomer orbitals is exactly analogous to that used in analysis of π systems of conjugated linear olefins.[13] Taking the combined splitting of the $a_{1g}(dz^2)$ and $a_{2u}(\pi^*)$ orbitals between dimers as β, the Huckel predictions for energies of the lowest band are $E_{D_2} = E_D + \beta$, $E_{D_3} = E_D + \sqrt{2}\,\beta$, $E_{D_4} = E_D + \frac{(1+\sqrt{5})}{2}\,\beta$, where $E_D = E(1a_{2u} \rightarrow 2a_{1g})$. For $\beta = 5500\ cm^{-1}$, theory and experiment agree quite well as shown in table 3.

The broad absorption centered at 1735 nm (5760 cm^{-1}) and present only at the highest concentrations probably represents overlapping bands due to higher oligomers ($n > 4$), as the calculated limit for $n = \infty$ is $E_D + 2\beta$, or 7000 cm^{-1}.

Table 3

Calculated transition energies for $(Rh_2(bridge)_4^{2+})_n$ from Huckel theory.

Assumed a value for β of 5500 cm^{-1}.

n	Calculated Energy [a]	Observed Energy [a]
1	-----	18,000
2	12,500	12,820
3	10,220	10,080
4	9,100	8,770

a) all energies in cm^{-1}.

Oxidative Addition Reactions

In addition to the unique electronic features which are a consequence of the strong coupling between metals in $Rh_2(bridge)_4^{2+}$, the orbital interactions in the dimer also promote unusual redox processes not found in monomeric or weakly coupled dimeric systems. A prime example of this coupling is the oxidative addition of molecular halogens across the rhodium-rhodium axis, resulting in the trans dirhodium(II) adducts $Rh_2(bridge)_4X_2^{2+}$ (X=Cl, Br, I) with halide atoms occupying axial positions and formation of a metal-metal bond between the rhodiums. This new type of two-center, two electron oxidative addition process is in sharp contrast with the conventional one center oxidative additions common to most square planar d^8 systems (including the $Rh(CNR)_4^+$ monomers).[14] The oxidative addition reactions undergone by $Rh_2(bridge)_4^{2+}$ are wide and varied, and substrates include Cl_2, Br_2, I_2, CH_3I, C_2H_5I, NO, $P(OCH_3)_3$, methyl tosylate and O_2(weakly). Shortly after the communication of this redox system, similar two-center oxidation processes with halogens have been found to occur on a variety of dimeric rhodium(I) systems by other workers[15], and it appears that the reactions may turn out to be quite general in nature and not restricted merely to rhodium systems.

Upon addition of X_2 (X=I, Br, Cl) to solutions of $Rh_2(bridge)_4^{2+}$, striking changes take place in the electronic absorption spectrum. These changes are similar for all the halogens; however, due to ease of handling, most of the results to be discussed below were obtained for the I_2 adduct.

As shown in figure 14, when I_2 is added to dilute solutions of $Rh_2(bridge)_4(BPh_4)_2$ in acetonitrile, pronounced spectral changes are observed to

occur until two equivalents of I^- have been added to the solution. The oxidative adduct formed at this endpoint contains two Rh(II)-I units connected by a single metal-metal bond. The infrared spectrum of a KBr pellet of $(Rh_2(bridge)_4I_2)(I_3)_2$ (the product is isolated as a triiodide salt resulting from I_2 oxidation of BPh_4^-) exhibits a single C≡N stretch at 2227 cm^{-1}, indicating trans I-Rh-Rh-I stereochemistry, and the higher $\bar{\nu}$ (C≡N) frequency observed for $Rh_2(bridge)_4I_2^{2+}$ as compared to that of $Rh_2(bridge)_4^{2+}$ is consistent with the formulation as proposed above.

The electronic absorption spectra of the oxidative addition adducts may be interpreted in terms of our previous MO formulation of the metal-metal interaction in $Rh_2(bridge)_4^{2+}$. Upon oxidation, the two electrons in the antibonding $1a_{2u}$ orbital are transferred to the two iodine atoms to yield two I^- groups and a Rh(II)-Rh(II) bond with the configuration $(1a_{1g})^2$. The electronic absorption spectrum of $Rh_2(bridge)_4I_2^{2+}$ in acetonitrile solution exhibits intense bands at 465 nm(ϵ=23,000) and 397 nm (ϵ=62,000). The very intense 397 nm band is logically attributable to the $\sigma\rightarrow\sigma^*$ transition ($1a_{1g} \rightarrow 1a_{2u}$) in the Rh(II)-Rh(II) singly bonded species, as intense $\sigma\rightarrow\sigma^*$ bands in this energy region have been observed for $Mn_2(CO)_{10}$ as well as numerous other d^7-d^7 metal-metal- bonded systems.[16] The band at 465 nm could be due to one or more $d\pi\rightarrow\sigma^*(1a_{2u})$ transitions, again by analogy to $Mn_2(CO)_{10}$. The intense bands in the corresponding bromo- and chloro- adducts presumably represent the $d\pi\rightarrow\sigma^*$ and $\sigma\rightarrow\sigma^*$ transitions in these adducts. The small blue shift in the position of the $1a_{1g}\rightarrow 1a_{2u}$ transition for the series of $Rh_2(bridge)_4I_2^{2+}$ to $Rh_2(bridge)_4Br_2^{2+}$ to $Rh_2(bridge)_4Cl_2^{2+}$ is consistent with some fractional charge transfer character, as it is reasonable to expect that the $1a_{1g}$ orbital will be

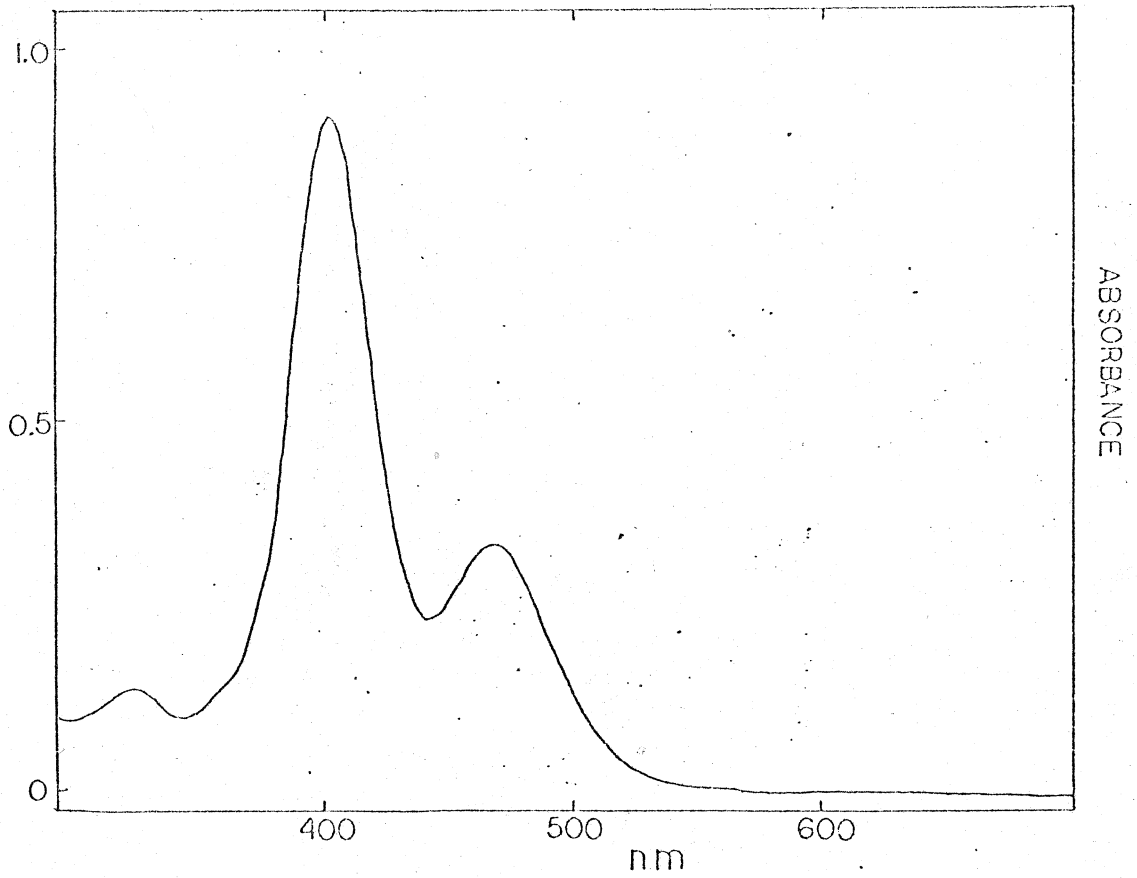

Figure 11

Electronic absorption spectrum of $Rh_2(bridge)_4I_2^{2+}$ in CH_3CN.

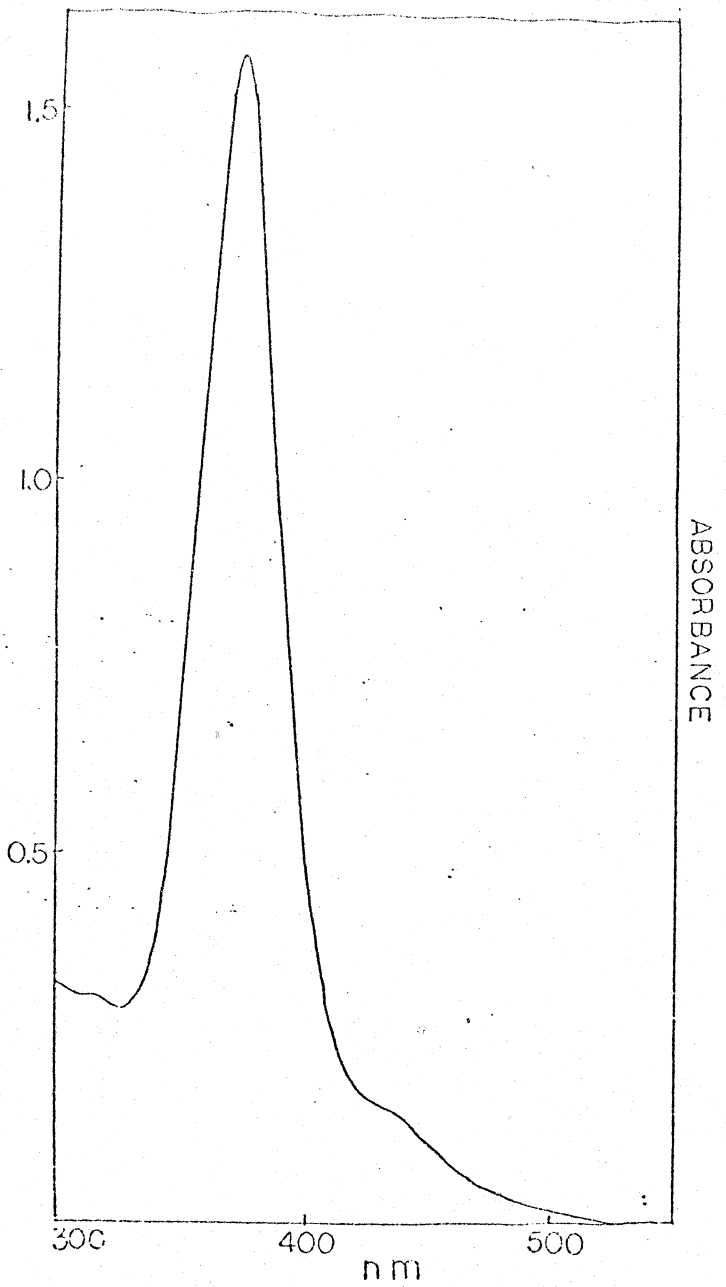

Figure 12

Electronic absorption spectrum of $Rh_2(bridge)_4Br_2^{2+}$ in DMF.

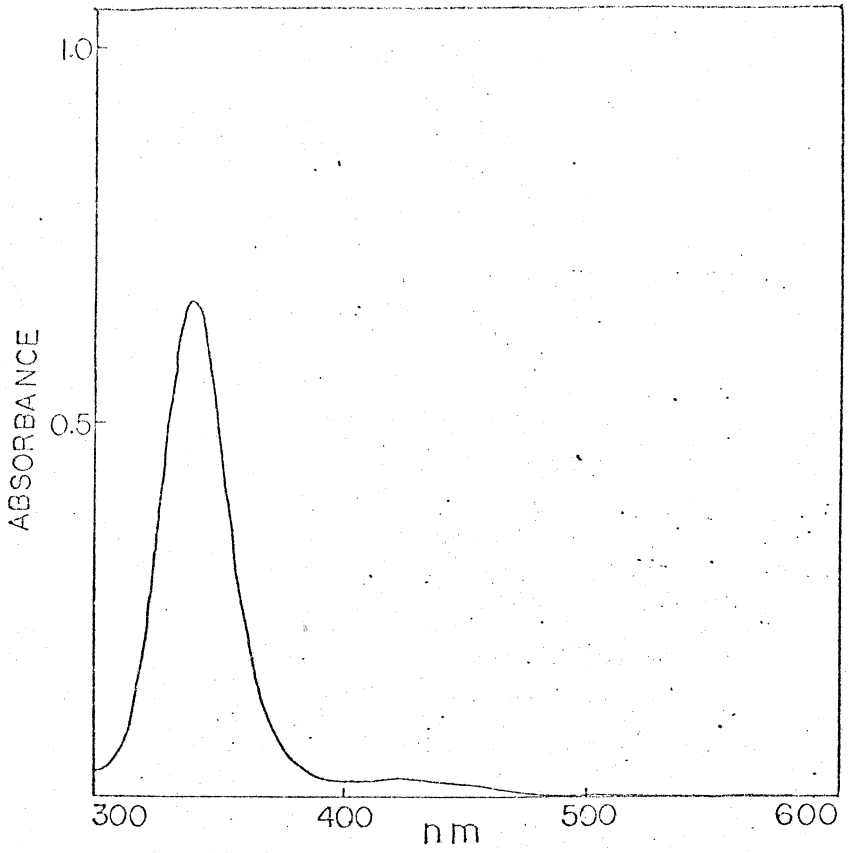

Figure 13

Electronic absorption spectrum of $Rh_2(bridge)_4Cl_2^{2+}$ in CH_3CN.

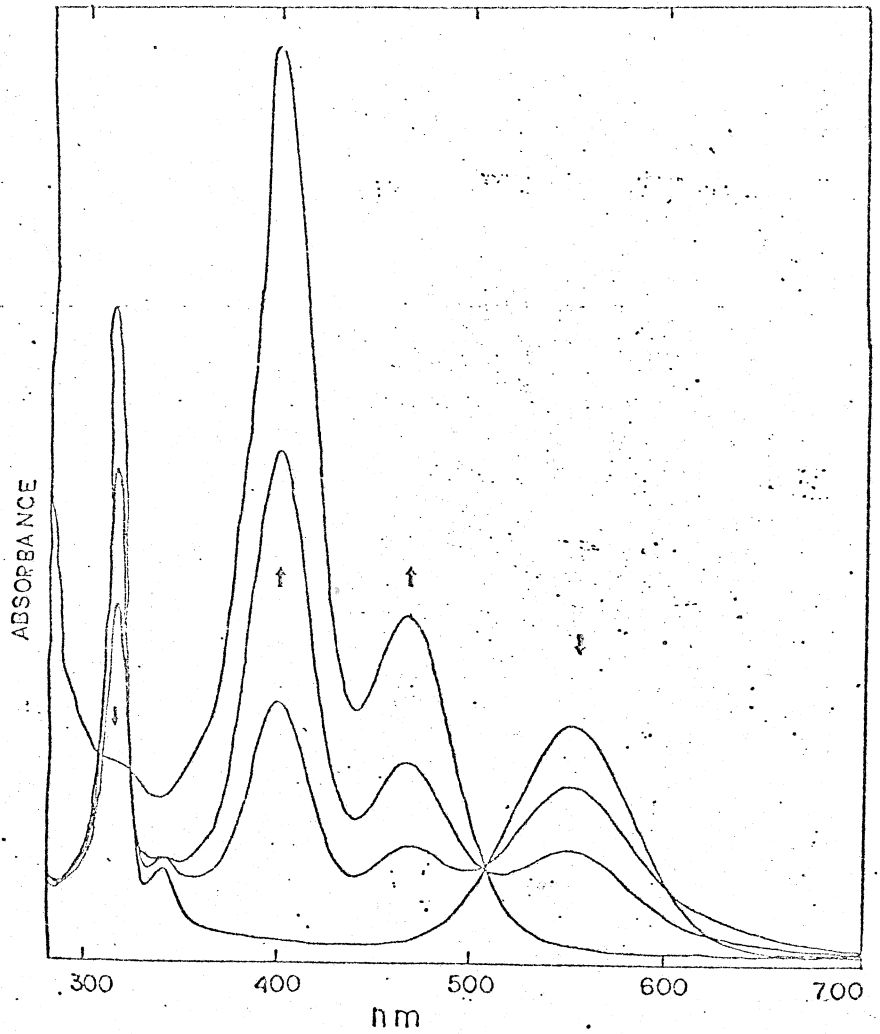

Figure 14

Titration of $Rh_2(bridge)_4(BPh_4)_2$ with I_2 in CH_3CN.

delocalized to some extent over the entire X-Rh-Rh-X framework.

When the I_2 oxidation was performed at high concentrations of $Rh_2(bridge)_4^{2+}$, a green intermediate species was observed with a band maximum at 626 nm. The concentration of this species maximized at the stoichiometric ratio of 2 $Rh_2(bridge)_4^{2+}$ to one I_2, and unlike $Rh_2(bridge)_4^{2+}$ and $Rh_2(bridge)_4I_2^{2+}$, the absorbance due to this intermediate did not follow Beer's law. Rather, detailed concentration dependences as shown in figure 16 indicate that the concentration of this intermediate is proportional to the square of the $Rh_2(bridge)_4^{2+}$ concentration. The green species is therefore logically formulated as a partially oxidized dimer-of-dimers, e.g. $I\text{-}Rh^{II}\text{-}Rh^{I}\text{-}Rh^{I}\text{-}Rh^{II}\text{-}I$. Similar behavior was observed for the Br_2 oxidation (but not for the Cl_2 reaction), yielding a species with λ_{max} of 597 nm in DMF solution. For both these reactions, the intermediates are not isolatable, as they disproportionate to starting material and final product upon attempted precipitation. Certainly, the available spectral data are consistent with the proposed formulation, however, we may not conclusively rule out the possibility of a bridging I^- moiety or some other partially oxidized structure for this intermediate.

One of the most interesting features of this oxidative addition with halogens is the facile thermal reversibility of the Br_2 and Cl_2 adducts. When solutions of $Rh_2(bridge)_4Br_2^{2+}$ in acetonitrile or DMF-water mixtures are heated, complete conversion to $Rh_2(bridge)_4^{2+}$ is obtained, and the unoxidized material may be recovered by precipitation or quantitavely reoxidized upon further addition of bromine. Similar behavior was observed for the Cl_2 reaction, and in both cases the reaction may be cycled several times without detectable loss of material.

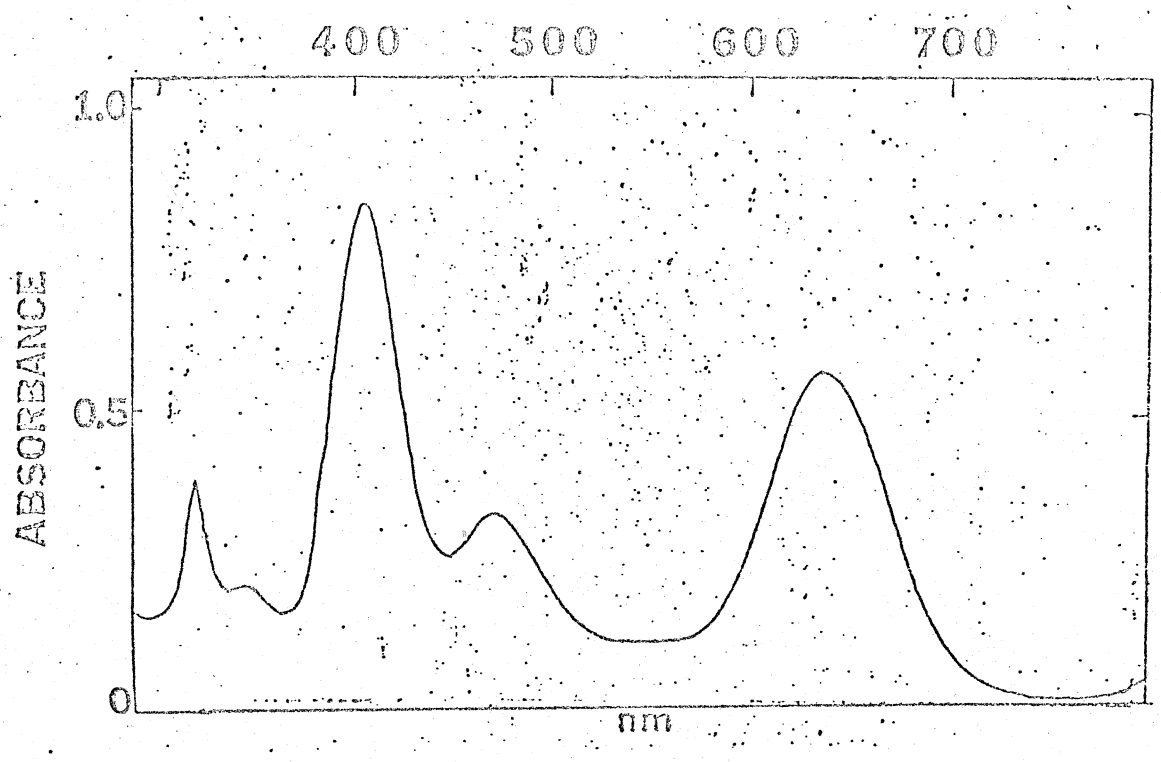

Figure 15

Typical point in the titration of I_2 with $Rh_2(bridge)_4(BPh_4)_2$ in CH_3CN; titration was performed at very high Rh concentrations (10^{-3}M).

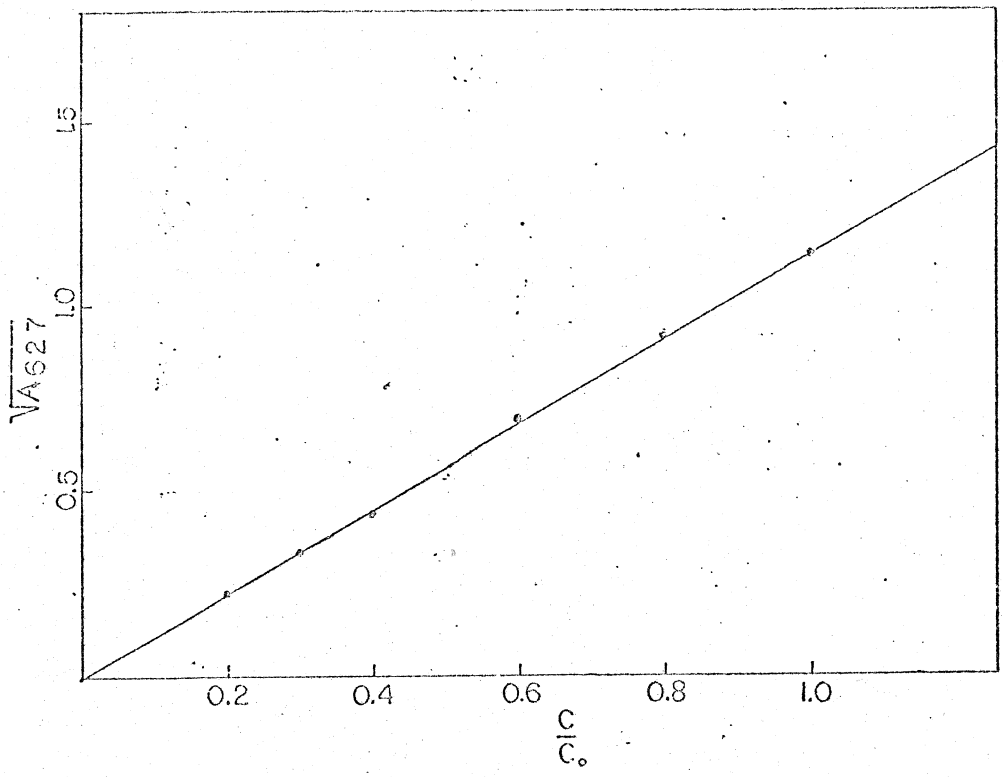

Figure 16

Plot of square-root of 626 nm absorbance vs. initial dimer concentration in titration with I_2 in CH_3CN.

The anomalous behavior exhibited by the irreversibility of $Rh_2(bridge)_4I_2^{2+}$ is interpreted as the inability to rapidly purge the solutions of I_2, but boiling of solvent is sufficient to assure that Br_2 and Cl_2 will escape from the solution before reoxidizing $Rh_2(bridge)_4^{2+}$. The I_2 irreversibility also reflects an increased stability of $Rh_2(bridge)_4I_2^{2+}$ over the bromo- and chloro- adducts, as would be expected for addition of softer ligands to a soft rhodium(I) complex.

In order to gain additional stereochemical information and greater spectroscopic probes into the mechanism of oxidative addition, the oxidation of $Rh_2(bridge)_4^{2+}$ with an unsymmetrical adduct, methyl iodide, was investigated. Facile oxidation of acetonitrile solutions of the $Rh_2(bridge)_4(BPh_4)_2$ complex may be accomplished be addition of methyl iodide, which leads to an adduct which may be isolated as reddish brown crystals by slow addition of diethyl ether. This reaction, like the Br_2 and Cl_2 oxidations, is also thermally reversible under mild conditions, and exhibits similar cycling properties upon the thermal purging of methyl iodide from the solution. The 60-MHz PMR spectrum of this species in DMSO exhibits broad multiplets at 4.0, 2.1, and 1.3 δ (in addition to the tetraphenylborate, water, DMSO, and acetonitrile protons). As the resonance at 1.3 ppm does not correspond to any feature in unoxidized $Rh_2(bridge)_4^{2+}$ or CH_3I, it is therefore attributed to a methyl group bonded to rhodium. Other examples of proton chemical shifts in similar monomeric systems also occur in this same vicinity for a variety of metal-CH_3 adducts. Furthermore, the observation of a 1-2 Hz splitting of this resonance into a doublet attributable to coupling with the ^{103}Rh nucleus confirms the assignment proposed above.

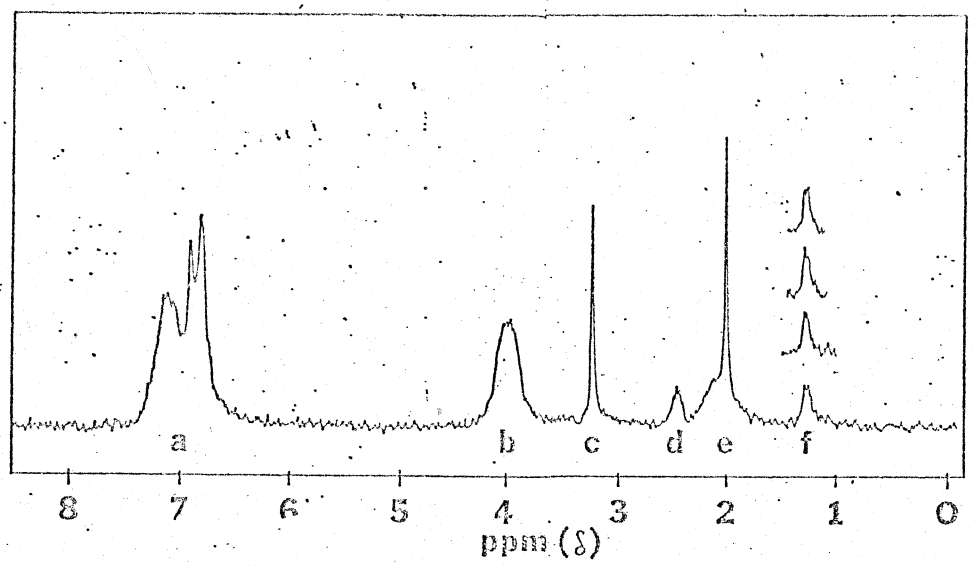

Figure 17

60 MHz PMR spectrum of $Rh_2(bridge)_4(CH_3)(I)^{2+}$.

The infrared spectrum of the methyl iodide adduct exhibits two ν(C≡N) stretches, as expected, both intermediate in position between the bands in $Rh_2(bridge)_4I_2^{2+}$ and $Rh_2(bridge)_4^{2+}$. These positions are consistent with one Rh(II)-like nucleus (bonded to I^-) and one Rh(I) type center (bonded to CH_3), as is expected for the trans stereochemistry.

Although the infrared spectrum of $Rh_2(bridge)_4(CH_3)(I)^{2+}$ shows characteristics intermediate between those of $Rh_2(bridge)_4I_2^{2+}$ and of $Rh_2(bridge)_4^{2+}$, the electronic absorption spectrum of $Rh_2(bridge)_4(CH_3)(I)^{2+}$ closely resembles that of the diiodo adduct, and exhibits bands at 397 nm and 470 nm in acetonitrile solution. These transitions are logically assigned to the $\sigma \rightarrow \sigma^*$ and $d\pi \rightarrow \sigma^*$ transitions, by analogy to the $Rh_2(bridge)_4X_2^{2+}$ adducts. The strong resemblance of the $Rh_2(bridge)_4(CH_3)(I)^{2+}$ adduct to $Rh_2(bridge)_4I_2^{2+}$ in the electronic absorption spectrum is again consistent with the $1a_{1g} \rightarrow 1a_{2u}$ transition possessing some charge transfer character due to mixing of I^- p orbitals along the Rh-Rh axis.

There has been much interest in the mechanism of oxidative addition, and several theories have been proposed to explain the data for the one-centered additions.[17-20] Perhaps the most perplexing result is the wide occurrence of trans oxidative addition, both in monomeric and dimeric systems. Even with highly hindered macrocycles in monomeric systems, where a concerted addition or any type of intramolecular rearrangement may be ruled out on the basis of steric factors, exclusively trans addition is found to occur. Furthermore, in methyl iodide additions where excess labelled I^- is present, no inclusion of labelled iodine is found in the final oxidative adducts. Due to the modest rate of reaction and large changes in the visible absorption spectrum, the oxidation of $Rh_2(bridge)_4^{2+}$ with methyl iodide

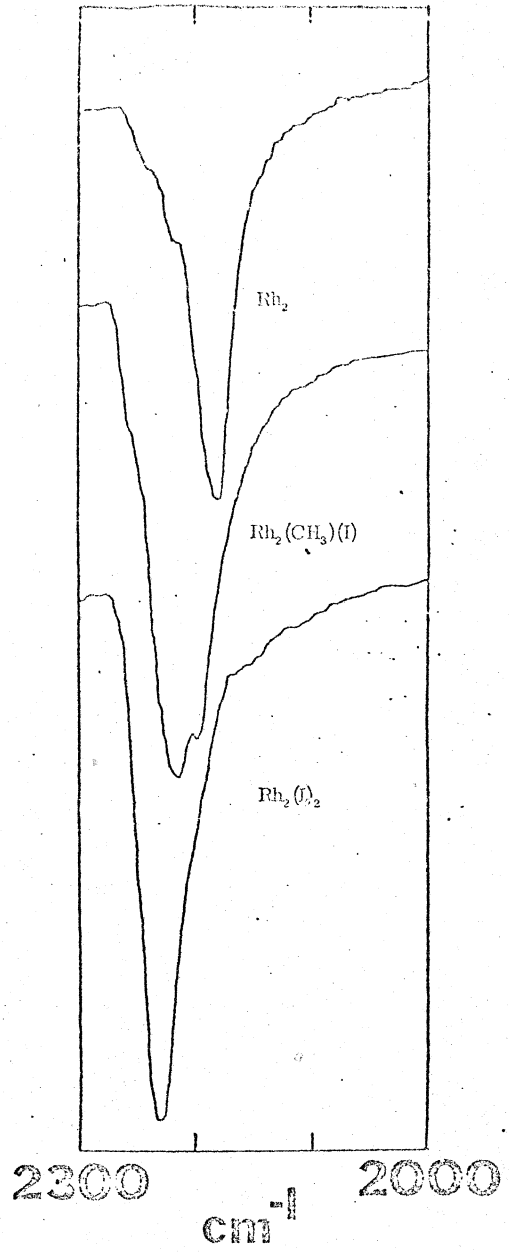

Figure 18

Infrared spectra of $Rh_2(bridge)_4^{2+}$, $Rh_2(bridge)_4(CH_3)(I)^{2+}$, and $Rh_2(bridge)_4I_2^{2+}$ as KBr pellets.

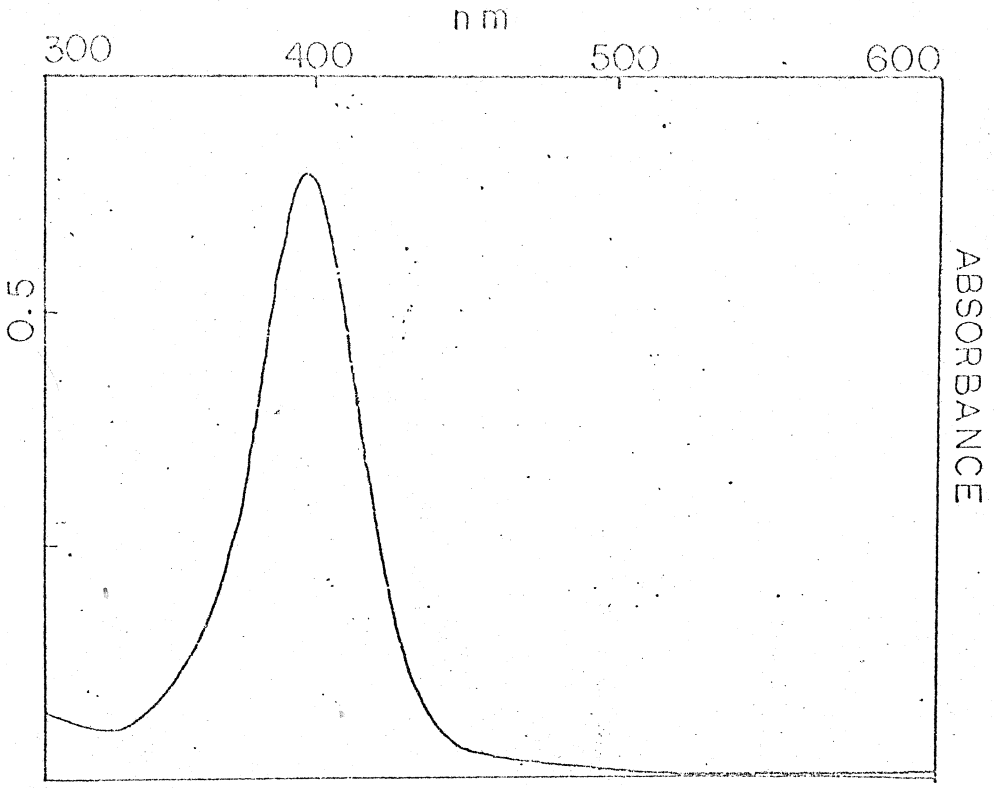

Figure 19

Electronic absorption spectrum of $Rh_2(bridge)_4(CH_3)(I)^{2+}$ in CH_3CN.

is ideally suited for spectroscopic study with a stopped-flow apparatus. To this end, several kinetic measurements were made on a rapid scanning spectrometer type stopped-flow apparatus, which allowed continuous monitoring of the entire visible spectrum. Rate data obtained in this fashion was for the disappearance of $Rh_2(bridge)_4^{2+}$, which was monitored at several wavelengths around 555 nm. Under pseudo-first order conditions in methyl iodide, the reaction is found to be strictly first order in $Rh_2(bridge)_4^{2+}$ for almost the entire reaction period, deviating only slightly in the final stages of sampling. These first order $Rh_2(bridge)_4^{2+}$ dependences were maintained over a wide range (factor of 100) of methyl iodide concentrations, with no apparent deviation even if the methyl iodide concentration is only a factor of five greater than the $Rh_2(bridge)_4^{2+}$ complex.

In order to determine the second order rate constant, a plot of methyl iodide concentration versus the observed rate constant was made; however this plot did not display the straight line expected for simple second order kinetics. Rather, the rapid saturation indicated the possible operation of a pre-equilibrium mechanism, and the appropriate Michaelis-Menten plot of inverse methyl iodide concentration versus the inverse of the observed rate constant was made. Again, no linear dependence was found, with the data deviating from linearity both at high and low concentrations (the curve actually looks as though it has two inflection points).

The approximate second order rate constant obtained by least-squares fitting of the data in the Michaelis-Menten plot is $3.67\ M^{-1}\ sec^{-1}$. This rate compares favorably to rates of between 10^{-2} and 10^{-3} found [14] for similar oxidative additions of methyl iodide to monomeric systems.

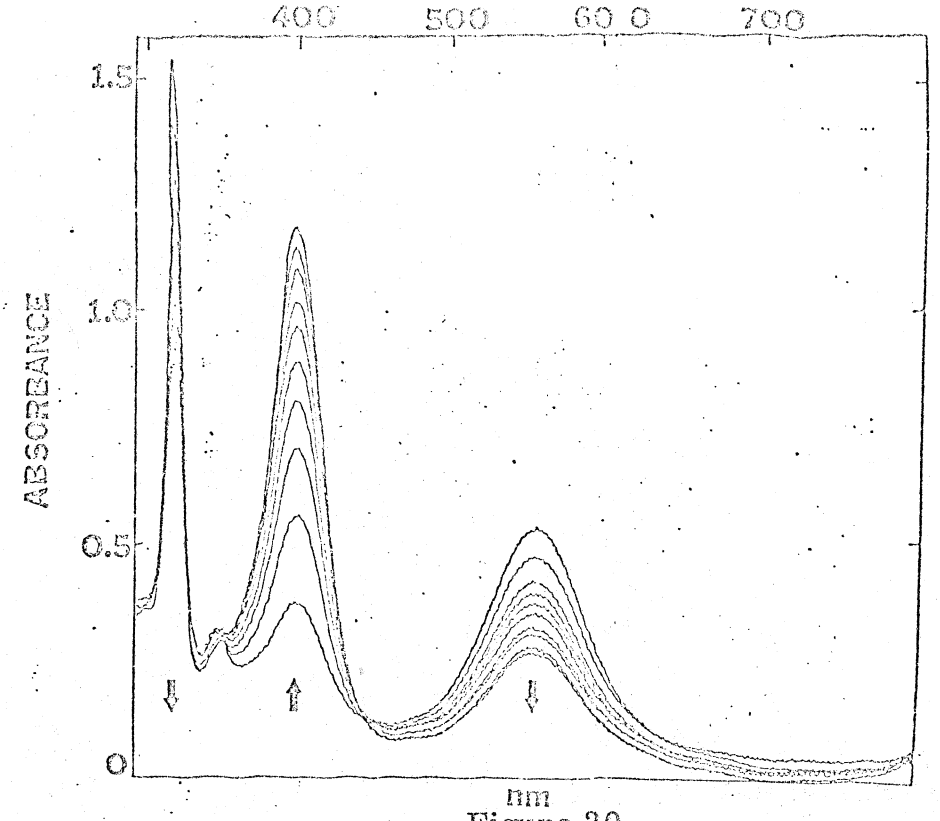

Figure 20

Typical spectral kinetics data for the addition of CH_3I to $Rh_2(bridge)_4(BPh_4)_2$ in CH_3CN.

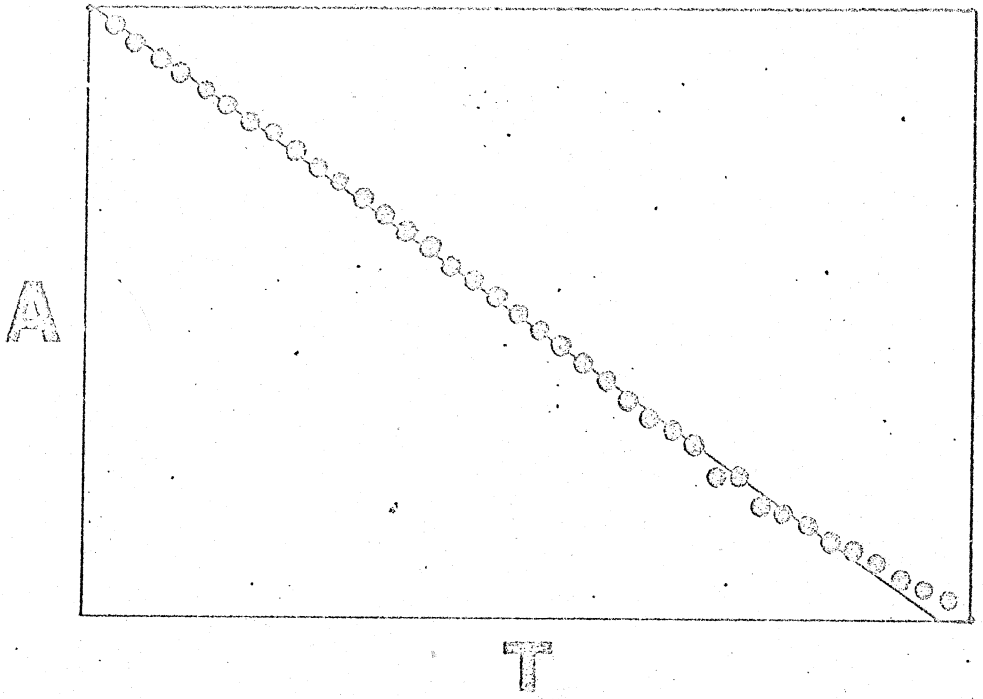

Figure 21
Typical plot of decay of dimer absorbance at 555 nm vs. time.

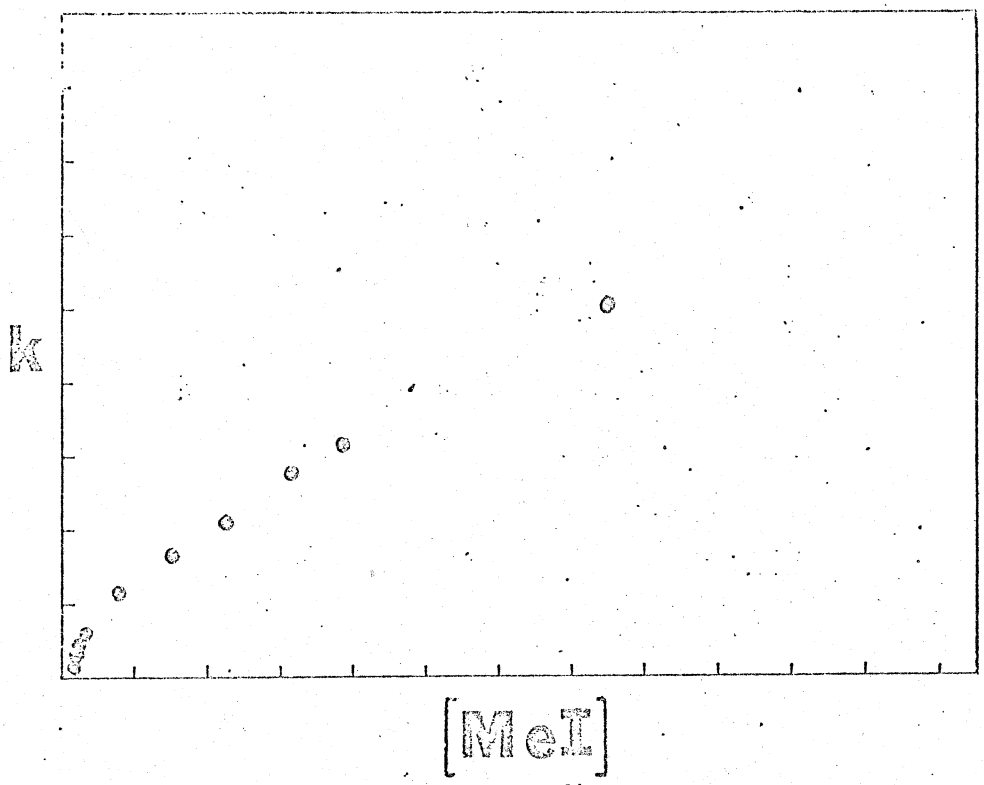

Figure 22

Plot of methyl iodide concentration vs observed rate constant. For strictly first order kinetics, this plot should yield a straight line.

Further kinetic studies indicate that the rate of ethyl iodide addition to $Rh_2(bridge)_4^{2+}$ is comparable to that of methyl iodide, and that methyl tosylate reacts extremely slowly. As the methyl tosylate data preclude the operation of a nucleophilic attack on carbon, it is suspected that the initial step involves rhodium attack on a heavy atom in the substrate, yielding $Rh_2(bridge)_4I^{2+}$ and methyl radicals in the case of methyl iodide. Certainly a free radical mechanism is suggested by the data presented, however the nature of the intermediate is still speculative. Other possibilities consistent with the data could include the $I\text{-}Rh^{II}\text{-}Rh^{I}\text{-}Rh^{I}\text{-}Rh^{II}\text{-}I$ species postulated as the stable intermediate in the I_2 oxidative addition, or a cooperative mechanism in which one metal center assists the other in the oxidative addition process; however, at this time, there is no basis for favoring any of the possible alternatives as probable intermediates.

Protonation Reactions

Although uncoordinated isocyanides are quite unstable in acid solution,[21] coordinated isonitriles exhibit exactly the opposite behavior and are stable at low pH but generate carbene complexes in neutral or basic solutions. Rhodium(I) isocyanide complexes are no exception to this rule, and are almost indefinitely stable in aqueous acid. While the rhodium(I) monomers exhibit no detectable chemical or physical changes in strong acid, dramatic effects are found to occur when the rhodium dimer $Rh_2(bridge)_4^{2+}$ is dissolved in aqueous acid. Surprisingly, the $Rh_2(bridge)_4^{2+}$ dication acts as a base, and reversibly binds protons in both aqueous and non-aqueous media. Due to the isocyanide ligands pushing electron density onto the rhodium atoms, the metals in the dimer are probably electron rich (at least for rhodium(I)) and might be reasonable bases. Furthermore, the polarization of electrons out of the center of the dimer causes increased electron density on the ends of the molecule, which also may contribute to the strong basicity of the complex. It is noteworthy that none of the equilibrium dimers formed by oligomerization of $Rh(CNR)_4^+$ monomers show any affinity for protons, and in this respect the $Rh_2(bridge)_4^{2+}$ dimer is truly unique.

Due to the instability of coordinated isocyanides under neutral or basic conditions (the half-life for $Rh_2(bridge)_4^{2+}$ at pH =7 is about thirty minutes), a full acid-base titration curve could not be obtained in aqueous solution. The stoichiometry of the protonation reaction was determined by monitoring the changes in pH when a known amount of $Rh_2(bridge)_4^{2+}$ was dissolved in slightly acidic solutions. The data, summarized in table 4 , indicate that the dimer picks up one proton in slightly acidic media. Though the equilibrium constant cannot be determined by this method, the observation that the $Rh_2(bridge)_4^{2+}$ ion

Table 4

Table of pH changes observed upon addition of fixed amounts of $Rh_2(bridge)_4(BF_4)_2$ to aqueous solutions.

Initial pH	Final pH	Theoretical Final pH[a]
3.88	4.10	4.14
3.75	3.85	3.85
3.75	3.99	4.02
3.77	3.87	3.89
3.77	4.12	4.21

a) Based on one proton per dimer, and using $\epsilon(DH)=52,000$.

is about 50% in the protonated form in pure water indicates that the pK_b is in the range of 6 to 7. Due to the striking spectral changes that occur on protonation (discussed in detail below), the stoichiometry could be checked by using the complex itself as an indicator. This spectrophotometric titration of $Rh_2(bridge)_4(BF_4)_2$ with para-tolunesulfonic acid in acetonitrile again verified the stoichiometry as one proton consumed per dimeric unit, as the proton balance in the spectrophotometric titration eliminates the possibility of any further protonations.[22]

Although the above chemical evidence definitely indicates that the dimer is indeed binding a proton, no proton NMR or infrared peaks have been found that are attributable to a metal-hydride bond, nor are there any spectral indications (except for the electronic spectrum as discussed below) that the ligand is not being protonated. Extensive Fourier transform 100 MHz PMR spectra were obtained for DMSO solutions 2:1 in para-tolunesulfonic acid to $Rh_2(bridge)_4(BF_4)_2$, taking over 10,000 transients over a range of 60 ppm, and no resonances attributable to any type of proton bound either to the metal or ligand were observed. The bridge ligand resonances themselves were similar to the unprotonated species but had slightly different chemical shift values. This verifies that some sort of non-destructive chemical change is occurring to the complex; unfortunately, it obviously does not provide any additional structural information.

The protonated species may be isolated by precipitation with ClO_4^-, CH_3COO^-, PF_6^- and other anoins, however, each of these salts yield irreproducible analyses and are undoubtedly impure. Efforts to purify the compound by recrystallization have failed; also the compounds bind irreversibly to all columns tried including alumina, silica gel, and

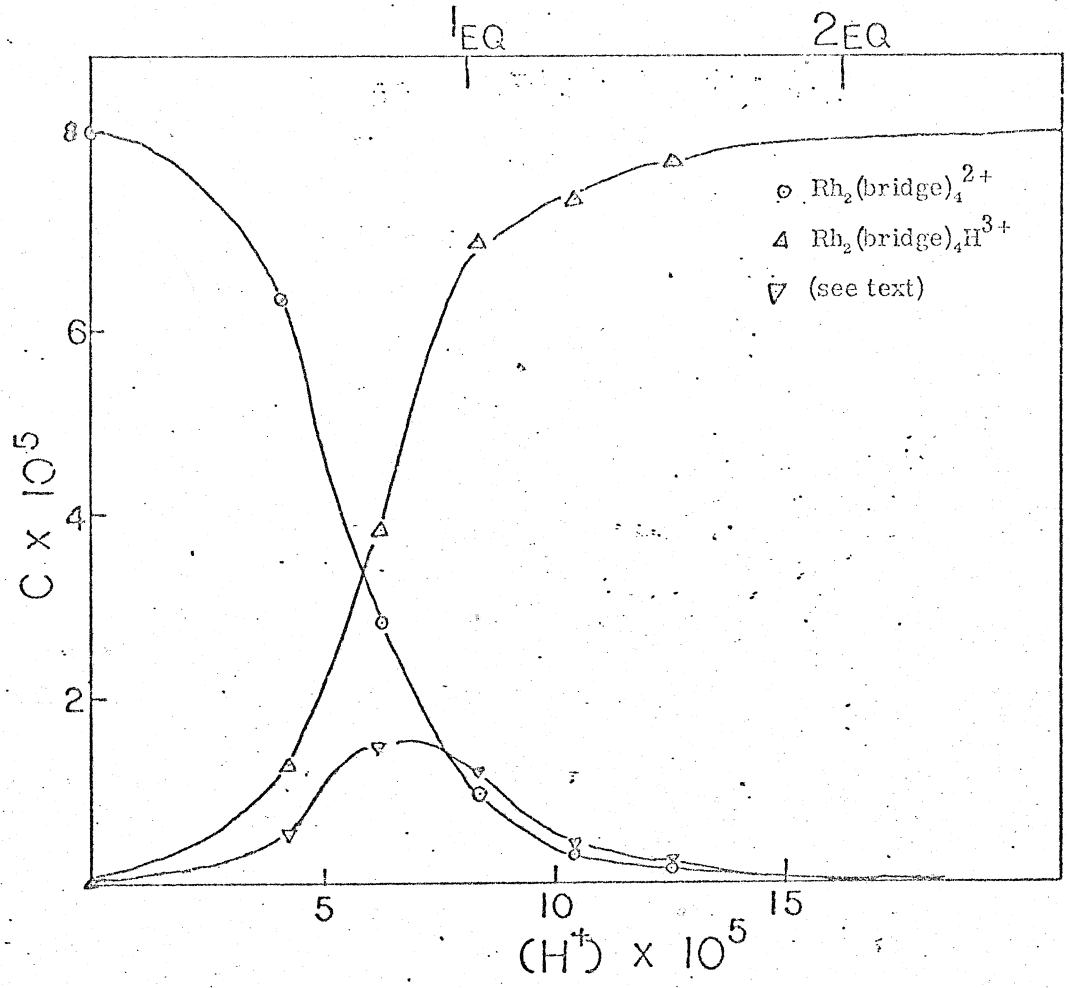

Figure 23

Titration of $Rh_2(bridge)_4(BF_4)_2$ with para-tolunesulfonic acid in CH_3CN.

Table 5

Data for Non-aqueous titration

Equivalents H^+	% as unprotonated form	% as fully protonated form
0	100	0
0.512	77.6	15.8
0.769	34.1	47.3
1.025	11.0	73.7
1.281	2.5	91.5
1.538	0.7	95.6
2.051	0.0	100.0

The unaccounted rhodium was assumed to be the intermediate species absorbing for a portion of the titration at 780 nm. (see footnote 22).

Sephadex G-10. These salts do redissolve to yield the correct absorption spectra, however their purity remains a serious problem. The infrared spectra as KBr pellets and Nujol mulls of the above salts, while hardly definitive, might provide some useful information: the $\nu(C\equiv N)$ stretching region shows one sharp band with a definite shoulder on the high energy side, and there are no bands attributable to modes corresponding to M-C=NHR functionalities. Furthermore, there are no band shifts upon deuteration which are not attributable to water stretching or bending modes. An indirect argument as to the location of the proton is that the $Rh(CNR)_4^+$ monomers do not react with strong acid, and this implies that the protonation is probably occurring at the metal in the dimer. All the evidence to date as to the location of the proton is indirect at best, and this issue is certainly unresolved at the present time (although chemical intuition, for all that it is worth, says that the proton is bonded to the metal).

The electronic spectrum of $Rh_2(bridge)_4^{2+}$ shows drastic changes upon protonation. The high energy (30,000 cm^{-1}) portion of the spectrum changes completely, while the low energy band does not shift much but shows over a threefold increase in intensity in acid solution. The spectrum is slightly anion dependent, however the major changes are observed only upon the addition of protons. The data summarized in table 6 show that the main spectral features are retained in all acids, and the anion dependence acts as a slight perturbation on the electronic structure. Jobe plots to determine anion stoichiometry have been performed for the case of chloride, and these results indicate one anion is strongly associated with the protonated dimer. The anion dependence is logically attributed to an axial

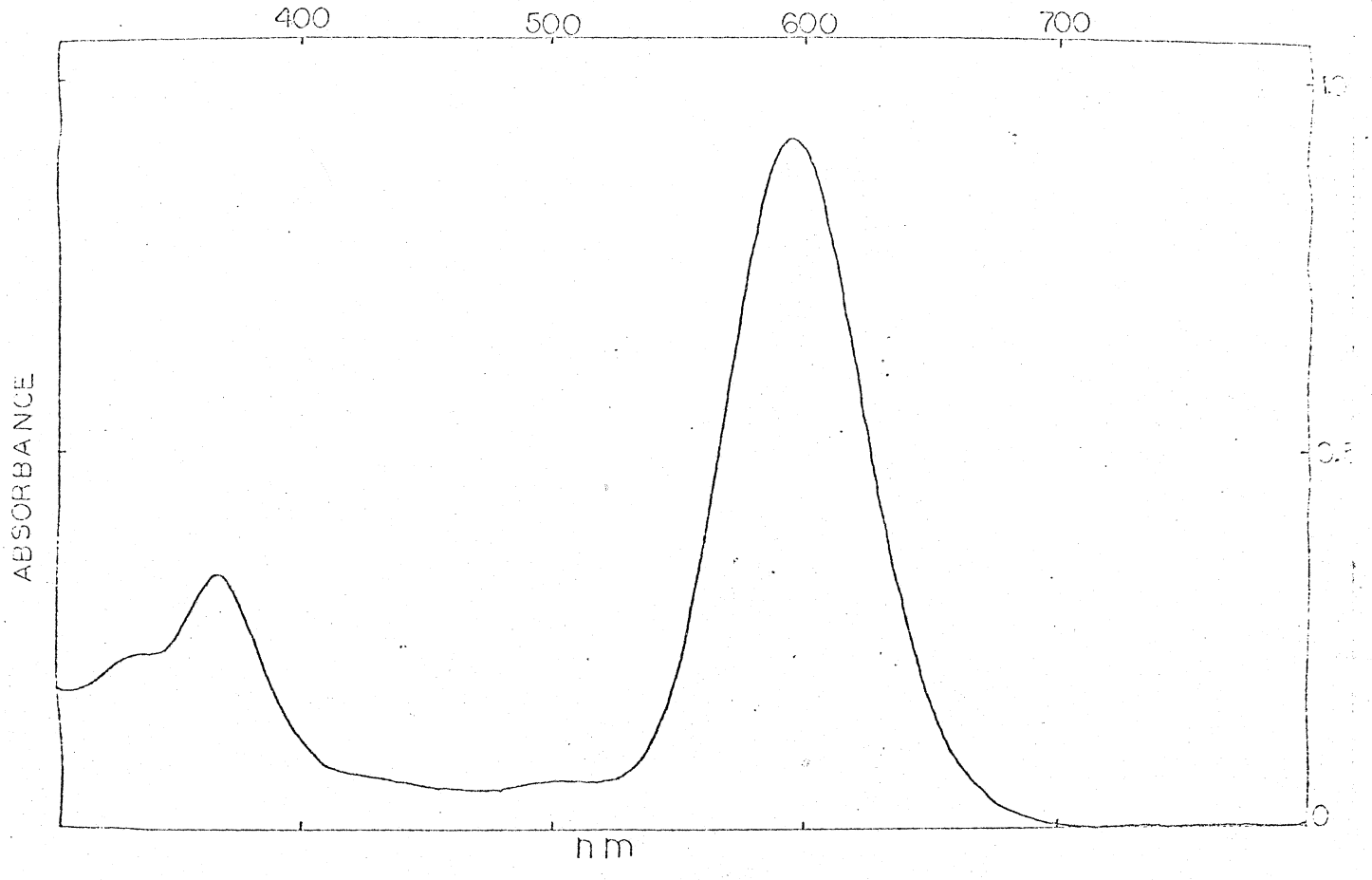

Figure 24

Electronic absorption spectrum of $Rh_2(bridge)_4^{2+}$ in 9 M HBr.

Table 6

Band maxima variation with anions

Band Maximum	Acid	Solvent
608	Tos	DMSO
592	HBr	H_2O
592	HBr	CH_3CN
578	HCl	H_2O
578	HCl	CH_3CN
551	Tos	CH_3CN

Tos=para-tolunesulfonic acid·1 H_2O

perturbation of the dσ Rh-Rh system, and from the data obtained we can establish a spectrochemical series for anion binding to protonated $Rh_2(bridge)_4^{2+}$ as follows:

$$DMSO < Br^- < Cl^- < CH_3CN$$

The similarity of this low energy transition to the $1a_{1g} - 2a_{1g}$ MLCT transition in $Rh_2(bridge)_4^{2+}$, the intense blue color of these complexes, and the facile deprotonation with base are all strong reasons as to the formulation of these species as protonated rhodium(I) compounds rather than rhodium(III) hydrides. To a certain extent, this counting of electrons is arbitrary; however, the principal electronic absorption of the protonated species is very near that of $Rh_2(bridge)_4^{2+}$, indicating a relatively small electronic perturbation has occurred upon protonation. In contrast, the related oxidative addition product of $Rh_2(bridge)_4(CH_3)(I)^{2+}$ exhibits its intense absorption at much higher energy and resembles $Rh_2(bridge)_4I_2^{2+}$ in its electronic structure. A similar protonation has been observed by Shaw[23] for $RhCl_2(PBu^tPr^n_2)_2$, which binds one proton to form a blue square-pyramidal-type complex.

Photochemistry

The methyl iodide oxidative addition product, $(Rh_2(bridge)_4(CH_3)(I))(BPh_4)_2$, undergoes an interesting photochemical reaction when irradiated with visible light ($\lambda \geq 310$ nm). Preliminary investigations indicate formation of the green partially oxidized species observed in I_2 oxidation of $Rh_2(bridge)_4^{2+}$ and postulated as $(Rh_2(bridge)_4I)_2^{4+}$, with subsequent formation of $Rh_2(bridge)_4^{2+}$ upon further irradiation. However, conversion with broad band irradiation is not clean, and the wavelength dependence of this photochemistry needs further investigation.

In contrast, when $Rh_2(bridge)_4^{2+}$ is dissolved in concentrated aqueous HBr or HCl, the blue protonated species previously discussed is immediately formed. Photolysis into the low energy intense bands[24] (either 546 nm light, or simply using a 520 nm cutoff filter) in degassed solutions leads to clean conversion to the $Rh_2(bridge)_4X_2^{2+}$ species previously prepared by thermal oxidation of $Rh_2(bridge)_4^{2+}$ [25]. The spectral changes during the photolysis are shown in figures 25 and 26. The reaction stoichiometry was verified to correspond to an overall two electron oxidation by monitoring the pH changes in undegassed acid during photolysis. These experiments indicate that the overall change from $Rh_2(bridge)_4^{2+}$ to $Rh_2(bridge)_4X_2^{2+}$ is 2.04 ± 0.05 electrons, as expected, while also verifying that one proton is consumed in the reaction of $(Rh_2(bridge)_4(H))^{3+}(X^-)$ to $Rh_2(bridge)_4X_2^{2+}$. Furthermore, the lack of H_2 production upon dissolution of $Rh_2(bridge)_4^{2+}$ in degassed 12 M HCl indicates that all the redox equivalents must be accounted for by species in solution, and thus verifies the overall charge of the protonated species as 3+.

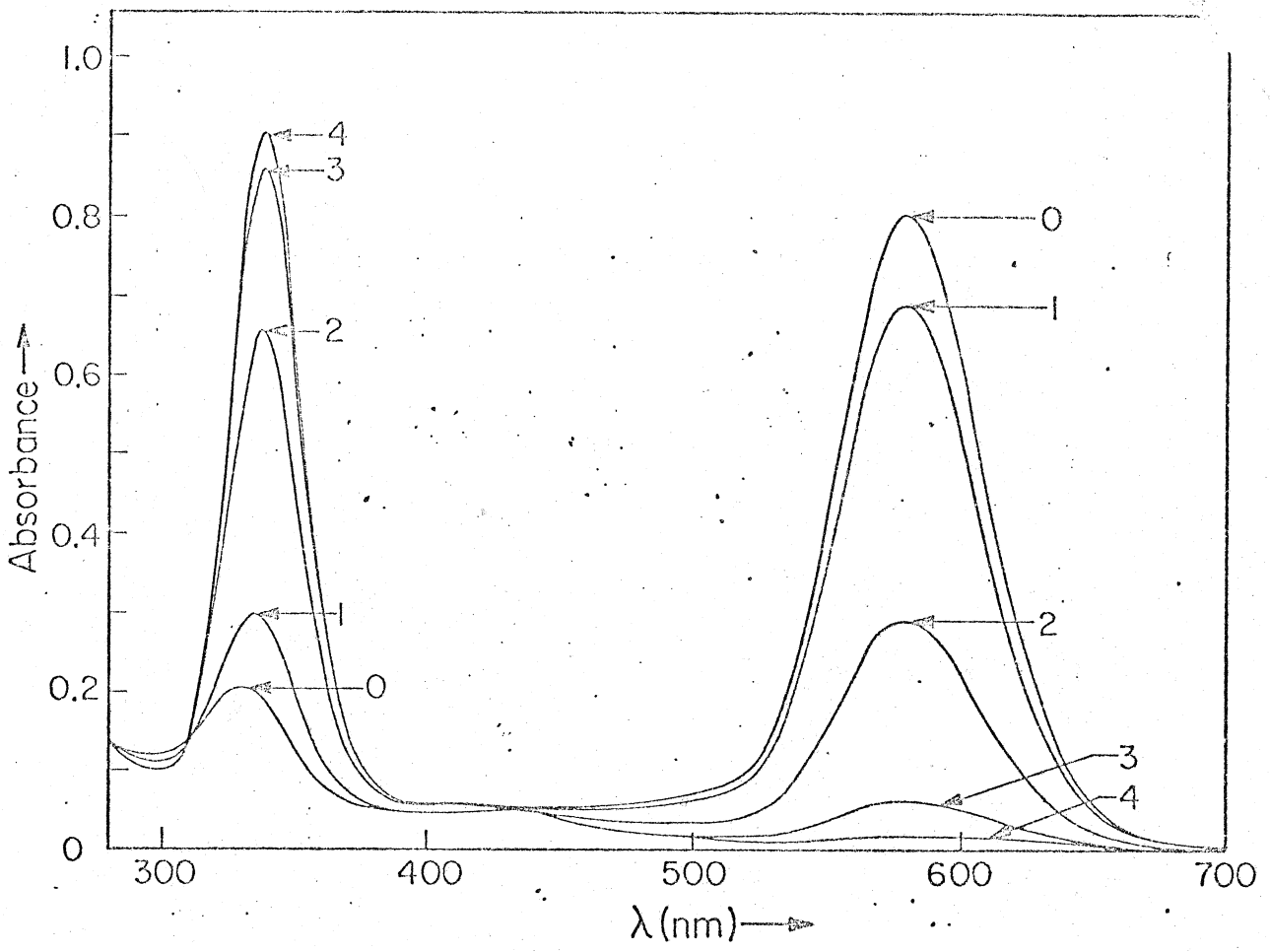

Figure 25

Degassed photolysis of $Rh_2(bridge)_4^{2+}$ at 546 nm in 12 M HCl. About 2 minutes between points.

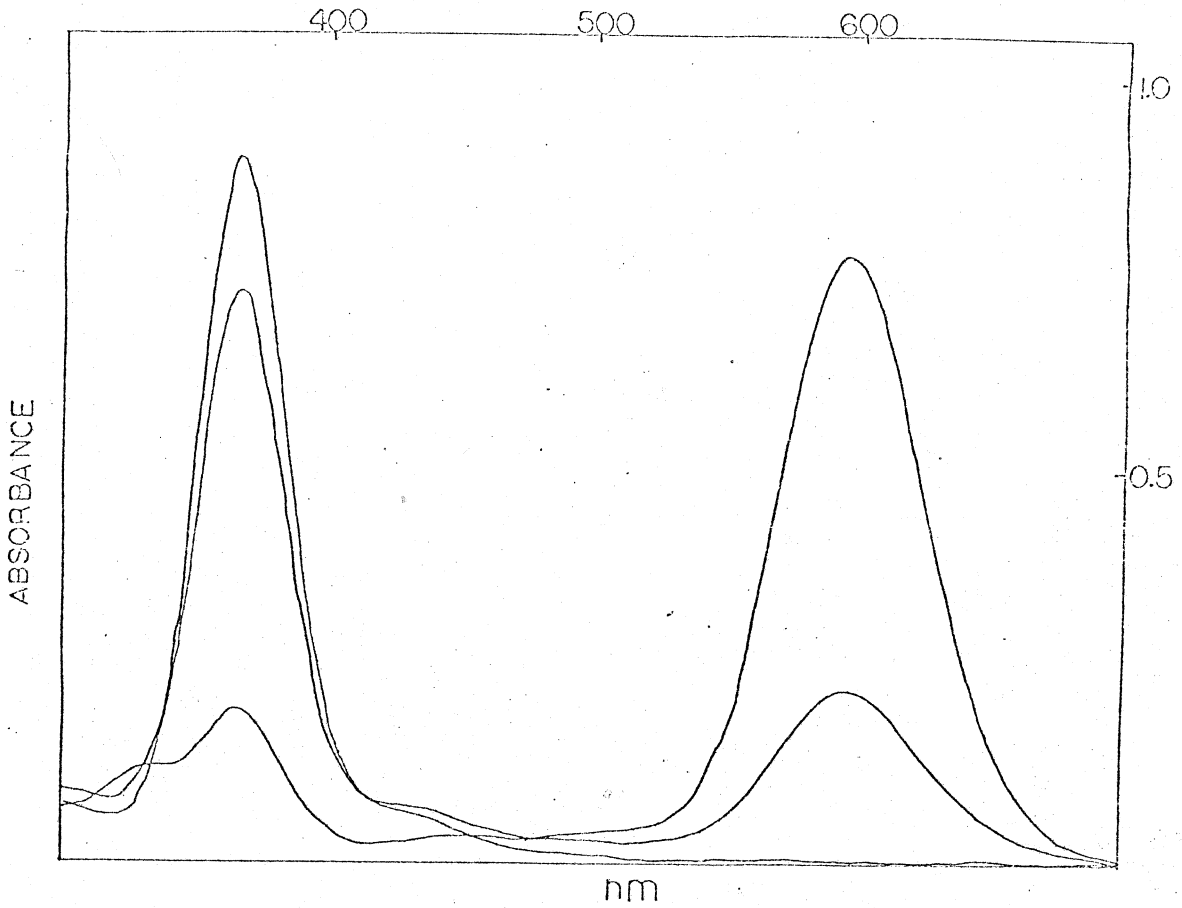

Figure 26

Degassed photolysis at 546 nm of $Rh_2(bridge)_4^{2+}$ in 9 M HBr. About 2 minutes between points.

Although quantum yield data indicate that the undegassed photoreaction corresponds to the reduction of O_2 to H_2O (table 7), degassed photolyses lead to production of hydrogen gas. This gas was collected by Toepler pumping and verified as H_2 both by burning over CuO and by mass spectroscopic analysis. In a typical experiment, conversion of 0.0567 mmol of $(Rh_2(bridge)_4(H))^{3+}(Cl^-)$ in 12 M HCl solution by irradiation at $\lambda \geq 520$ nm yielded 0.0466 mmol of H_2. The photoreaction is therefore formulated as follows:

$$\underset{\text{(blue)}}{(Rh_2(bridge)_4(H))^{3+}(Cl^-)} + H^+ + Cl^- \xrightarrow[12\ M\ HCl]{546\ nm} \underset{\text{(yellow)}}{Rh_2(bridge)_4Cl_2^{2+}} + H_2$$

The quantum yield of this reaction is highly anion dependent, changing from 0.004 in 12 M HCl to 0.04 in 9 M HBr. This is consistent with a mechanism in which axial interactions are necessary to stabilize the photoproduct $Rh_2(bridge)_4X_2^{2+}$. It is attractive to postulate that the axial binding serves as a barrier to back electron transfer and forces the two-electron photoreduction process to completion. Thus, it is proposed that the photoreaction occurs by the pathway shown below:

$$(\ (Cl^-)Rh^{I\frac{1}{2}} \text{---} Rh^{I\frac{1}{2}}(H^+)\ )^{2+} \xrightarrow{546\ nm} (\ Cl\text{-}Rh^{II} \text{---} Rh^{I}(H\cdot)\ )^{2+*}$$

$$(\ Cl\text{-}Rh^{II} \text{---} Rh^{I}(H\cdot)\ )^{2+*} \xrightarrow{fast} (\ Cl\text{-}Rh^{II}\text{-}Rh^{II}(H^-)\ )^{2+}$$

$$(\ Cl\text{-}Rh^{II}\text{-}Rh^{II}(H^-)\ )^{2+} + H_2O + Cl^- \xrightarrow{fast} (\ Cl\text{-}Rh^{II}\text{-}Rh^{II}\text{-}Cl)^{2+} + H_2 + OH^-$$

It is believed that the primary photoproduct arising from the $Rh\,dz^2 \rightarrow H\ 1s$ charge transfer excitation acts as if it were an activated hydride, e.g. LiH, NaH, etc., and will rapidly attack H_2O to transfer the first electron. However, without some method of inducing the second electron

Table 7

Quantum yield data for acid photolysis of $Rh_2(bridge)_4^{2+}$

All quantum yields are with 546 nm irradiation.

Acid	Concentration (M)	Φ	Degassed
HCl	1.20	0.032	N
HCl	1.09	0.031	N
HCl	0.11	0.028	N
HCl	0.012	0.011	N
HCl	12.0	0.002	Y
HBr	9.0	0.041	Y

to leave the metal, back electron transfer will occur, resulting in no overall reaction. Other systems with similar photoredox properties are found to undergo only one electron transfer unless some perturbation (usually in the form of a halide entering group) is present to induce the second electron transfer process. Thus, the axial stabilization provided by the entering halide ion is viewed as essential to the completion of the reaction, as without this stabilization there would be no facile mechanism for an efficient two-electron transfer process.

The photoreaction is uphill, as is evidenced by a slow thermal back reaction of $Rh_2(bridge)_4Cl_2^{2+}$ with H_2 in HCl to yield $Rh_2(bridge)_4(H)^{3+}$. Thus, this photoprocess could play a vital role in an energy conversion scheme, as it might be coupled with a process capable of oxidizing water to O_2. This would yield an overall decomposition of water into the storable energy sources of hydrogen and oxygen: $H_2O(l) \xrightarrow{h\nu} H_2(g) + O_2(g)$. Preliminary experiments with such an oxidant have been carried out and seem to be very favorable. The scheme under study involves the use of a polycrystalline TiO_2 electrode, which has been shown to be capable of oxidizing H_2O to O_2 upon irradiation with 366 nm light.[27] This oxidation process is achieved by photochemical excitation of an electron from the valence band of the material into the conduction band, resulting in a separated "electron-hole"pair (figure 27). With TiO_2 as the electrode, the electron hole in the valence band has the potential to oxidize water to yield oxygen, while the electrons excited into the conduction band flow through an external circuit, yielding the overall redox half-reaction:

$$TiO_2 + H_2O \xrightarrow{h\nu} TiO_2 + 1/2\ O_2 + 2H^+ + 2e^-$$

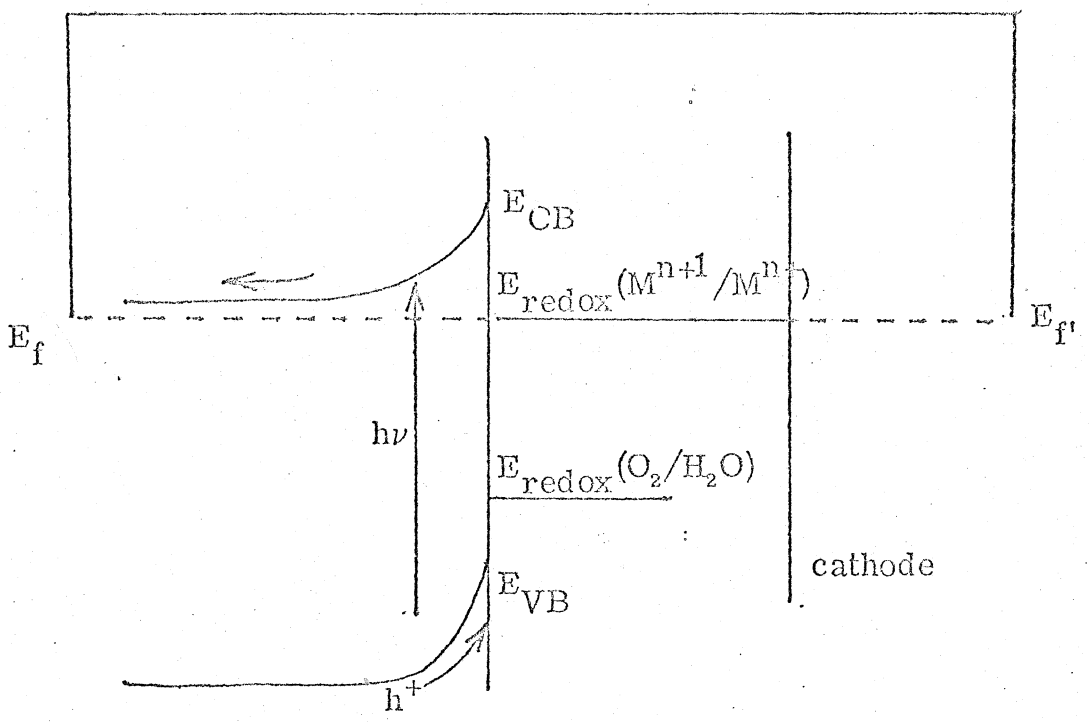

Figure 27

Ideal energetics for a TiO_2 photoelectrode. Electron holes in the valence band should be capable of oxidizing water, while the electrons in the conduction band should be able to regenerate the photoactive metal complex.

This reaction may be coupled to the $Rh_2(bridge)_4^{2+}$ photolysis in acid by use of the homogenous-heterogenous system depicted in figure 28. On one side of the diffusion barrier, TiO_2 is irradiated to produce O_2 and result in a current flow as described above. In the other side of the cell, $Rh_2(bridge)_4Cl_2^{2+}$ is reduced by the electrons on the platinum electrode to yield $(Rh_2(bridge)_4(H)^{3+})(Cl^-)$, which is then photolyzed to complete the cycle, yielding $Rh_2(bridge)_4Cl_2^{2+}$ and H_2. Cells of this type have been constructed, and preliminary experiments indicate that the cycling process may be carried out several times without detectable loss of material. However, when the reaction is carried out in aqueous HCl, another "super-reduced" species is observed to form in competition with reduction of $Rh_2(bridge)_4Cl_2^{2+}$, and thus serves to complicate the cycle. This "super-reduced" form may be oxidized back to $(Rh_2(bridge)_4(H))^{3+}(Cl^-)$ by application of an external oxidizing potential for a short period of time, and the cycle may then be reinitiated; however, this interruption of the cycle does not meet favorably with the desired continuous mode of operation. The corresponding photolysis in aqueous HBr does not seem to have these difficulties, and investigation of this process is underway at present.

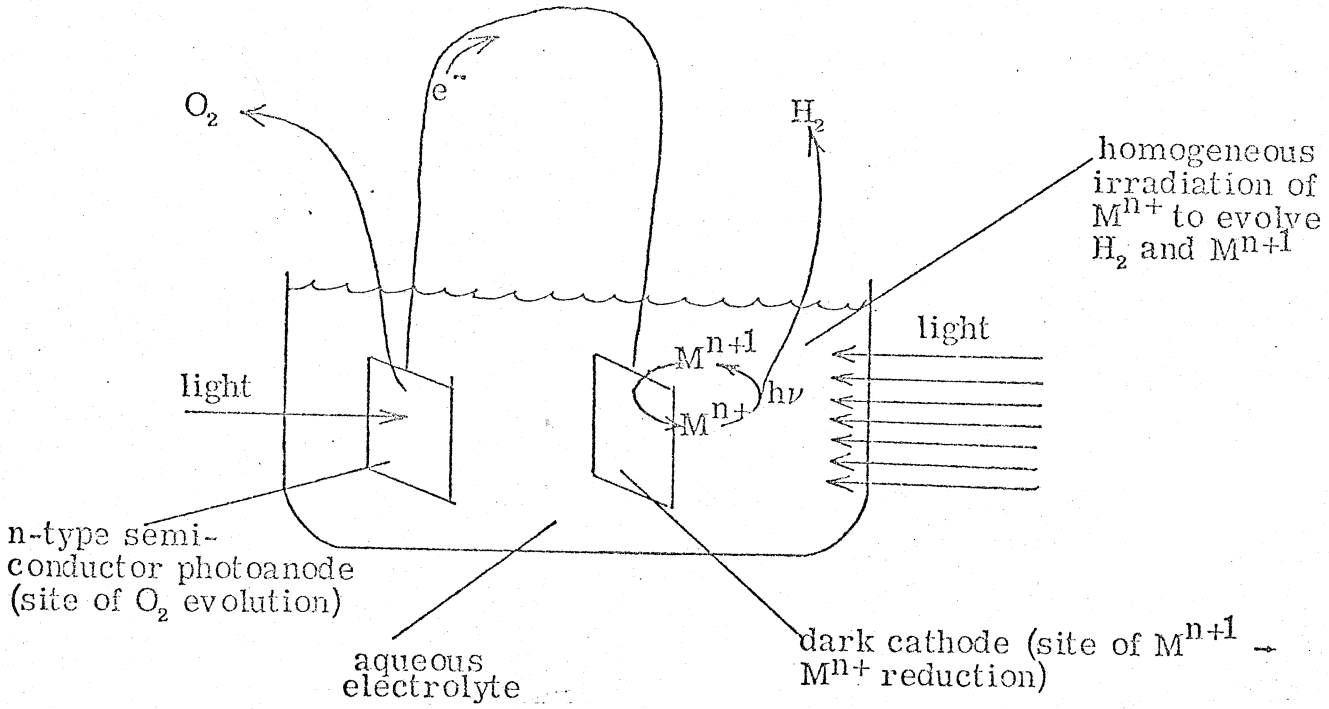

Figure 28

Prototype homogenous-heterogenous system for the solar conversion of water to H_2 and O_2. On the left side of the cell, is the O_2 producing TiO_2 photoelectrode, while the right side would contain $Rh_2(bridge)_4^{2+}$ in aqueous acid.

References

1. Kent Mann, Ph.D. Thesis, California Institute of Technology, 1976.
2. L. Malatesta and L. Vallarino, J. Chem. Soc., 1867 (1956).
3. K. R. Mann, J. G. Gordon, II, and H. B. Gray, J. Amer. Chem. Soc., 97, 3553 (1975).
4. K. R. Mann, N. S. Lewis, R. M. Williams, J. G. Gordon, II, and H. B. Gray, J. Amer. Chem. Soc., to be submitted for publication.
5. H. Isci and W. R. Mason, Inorg. Chem., 14, 913 (1975).
6. N. Lewis, unreported observations.
7. M. Olmstead and A. Balch, Inorg. Chem., in press.
8. This prediction was based on the fact that the low π_h^* level that is available in $Rh(CNPh)_4^+$ is not present in $Rh_2(bridge)_4^{2+}$. This leads to higher energy transitions in the alkyl case for a given Rh-Rh bond length, and correcting for this means that the bond lengths in $Rh_2(bridge)_4^{2+}$ and $(Rh(CNPh)_4)_2^{2+}$ should be similar, as indicated in the text.
9. J. N. Demas and G. A. Crosby, J. Amer. Chem. Soc., 93, 2841 (1971).
10. C. Lin and N. Sutin, J. Phys. Chem., 80, 97 (1976).
11. V. M. Miskowski, G. L. Nobinger, D. S. Kliger, G. S. Hammond, N. S. Lewis, K. R. Mann, and H. B. Gray, J. Amer. Chem. Soc., submitted for publication.
12. Similar behavior was also observed with $Rh_2(bridge)_4(BPh_4)_2$ in sulfolane.
13. A. Streitweiser, Jr., Molecular Orbital Theory for Organic Chemists, J. Wiley, New York, New York, 1961.
14. P. B. Chock and J. Halpern, J. Amer. Chem. Soc., 88, 3511 (1966).
15. A. L. Balch and M. M. Olmstead, J. Amer. Chem. Soc., 98, 2354 (1976).
16. R. A. Levenson and H. B. Gray, J. Amer. Chem. Soc., 97, 6042 (1975).

17. J. Chatt, L. A. Duncanson, and B. L. Shaw, Chem. Ind. (London), 859 (1958).

18. R. F. Heck, J. Amer Chem. Soc., 86, 2796 (1964).

19. F. Faraone, J. Chem. Soc., Dalton, 6, 541 (1975).

20. B. L. Shaw, J. Organomet. Chem., 94, 251 (1975).

21. J. U. Nef, Justis Liebigs Ann. der Chem., 270, 267 (1892).

22. During the non-aqueous titration, a species which has λ_{max} at 780 nm was observed to appear and then die away. This species may also be observed at high concentrations of $Rh_2(bridge)_4^{2+}$ in HCl and is probably a partially protonated oligomer.

23. C. Masters, B. L. Shaw, and R. E. Stainbank, Chem. Comm., 210 (1971).

24. A different reaction was observed with unfiltered light, leading to formation of an unidentified yellowish-brown solid.

25. During degassing, care must be taken to exclude mercury, as $(Rh_2(bridge)_4H)^{3+}(Cl)^-$ reacts with Hg to yield an air sensitive compound with λ_{max} of 410 nm. This species disproportionates to $(Rh_2(bridge)_4H)^{3+}(Cl)^-$ and $Rh_2(bridge)_4Cl_2^{2+}$ upon exposure to air.

26. K. R. Mann, H. B. Gray, and G. S. Hammond, J. Amer. Chem. Soc., 99, 306 (1977).

27. M. S. Wrighton, D. S. Ginley, P. T. Wolczanski, A. B. Ellis, D. L. Morse, and A. Linz, Proc. Nat. Acad. Sci., 72, 1518 (1975).

Molecular Orbital Calculations

In order to better understand the nature of the metal-metal interactions in the $(Rh(CNR)_4^+)_2$ dimers, an Extended-Huckel type molecular orbital calculation was performed. From this calculation, it was hoped that knowledge would be obtained about the significance of metal-metal overlaps, ligand orbital energies, and bond distances. To this end, calculations were performed on several monomers of the type $M(CNH)_4$, (M=Co(I), Rh(I), Ir(I), Ru(0), Pd(II)), and metal-metal overlaps for the corresponding dimers $(M(CNH)_4)_2$ were also found. In addition, full calculations were made on the $Rh_2(CNH)_8^{2+}$ and $Rh_2(CNH)_8Br_2^{2+}$ dimers. All metal-metal overlaps and full dimer calculations were performed at two metal-metal distances, 3.000 and 3.264 Å, in order to get a feel for how the results depend upon metal-metal bond length.

Method of the Calculation

All calculations were of the Extended-Huckel Self-Consistent Charge and Configuration type (EH-SCCC). In this method, discussed in detail by Ballhausen and Gray,[1] diagonal H_{ii} energy elements for the ligands are assumed as given, while the H_{ii} for the metal orbitals are taken as parametric functions of charge, the valence shell ionization energy curves (VSIE's). The off diagonal H_{ij} are set equal to $1/2(H_{ii}+H_{jj})FG$, where F is a fudge factor (usually about 2.00) and G is the appropriate group overlap. Full overlap matrices are calculated from the Slater-type atomic and molecular orbitals, and eigenvalues and eigenvectors are then obtained. A population analysis of the metal orbitals is performed, and the corresponding charge is compared to

the initial charge. The metal orbital energies are then readjusted to fit the new charge, and this cycle is reiterated until the charge and configuration have converged to self-consistency.

Since the calculation programs, Bev5 and Varif3, written by H. Basch at Columbia University in 1962, require that only three atoms be in the ligand, the CNR groups were modeled as CNH. Though several ab initio calculations have been performed on the CNH molecule, no data was available in the literature for wavefunctions with a Slater type basis set, so the ligand orbitals were also calculated using the same programs. However, the Varif3 program requires the metal to have d orbitals, so the nitrogen atom was taken as the metal with H and C as ligands, (bond lengths 0.97 and 1.17 Å, respectively) and hydrogen-like d orbitals were assumed for nitrogen in the calculation. Slater atomic basis sets and orbital energies were taken from Clementi.[2] VSIE's for nitrogen were available, and the program converged as normal despite the trickery involved. Though the wavefunctions obtained in this fashion were reasonable, the absolute energies were expected to be suspect, and upon comparison with ab initio calculations, this is found to be true.[3] For purposes of the metal complex calculations, the calculated wavefunctions were used and matched with the corresponding ab initio energies. (Calculations were actually done with both sets of energies, and the results, though fairly independent of ligand energies, seemed more reasonable for the ab initio energies) Monomers of the type $M(CNH)_4$ were then calculated for the five isoelectronic metals, Co(I), Rh(I), Ir(I), Ru(0). Pd(II), and fragments of H^+-$Rh^{I}(CNH)_4$ and Br-$Rh^{II}(CNH)_4$ were also calculated. Metal orbitals were taken from Richardson[4] for Co and from Basch and Gray[5] for the other metals.

VSIE's for first row metals were taken from H. Basch's Ph.D. thesis, while those for second and third row metals were approximated by subtracting 10,000 cm^{-1} from the C parameters. In order to then calculate the dimeric $(M(CNH)_4)_2$ molecules, metal-metal and certain ligand overlaps were calculated at 3.000 and 3.264 Å using the OVLAP program (3.264 Å is the observed Rh-Rh bond length in $Rh_2(bridge)_4(BPh_4)_2$ from the x-ray crystal structure--see appendix). The monomer fragments were then mixed by taking appropriate bonding and anti-bonding combinations for all orbitals, accounting for the splitting of these combinations by solving the appropriate two-by-two eigenvalue matrices, and then using the calculated overlaps to obtain eigenvalues and eigenvectors for the dimer. In this process, the monomeric metal charge, configuration, and orbital energies were used directly, and the diagonalization was performed only once, as the existing convergence routine is meaningless for a multi-metal system. The calculations were studied over a wide range of F factors (1.5 to 4.0) with many different combinations, and for consistency, all results discussed here have all F factors equal to 2.00, though in some cases better fits to experimental data could be obtained by choosing the F factors in a particular, but arbitrary, fashion.

Data and Results

Ligand wavefunctions and energies calculated for HNC are given in table 1, with ab initio energies included for comparison. Note that in changing from the HNC calculation to the $M(CNH)_4$ calculation, we must make the coordinate transformation Cz → -Cz, Cy → -Cy, Ny → -Ny in order to have all ligand atoms with left-handed coordinates.

Figure 1

Coordinate System used in calculations.

For the ligand orbital calculation:

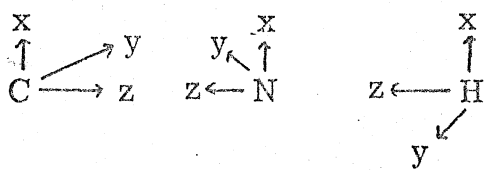

For the monomeric fragments:

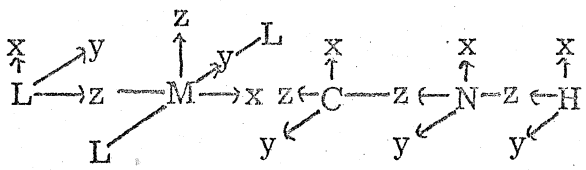

(The fifth ligand was placed on the positive z axis on the metal)

For the dimeric compounds:

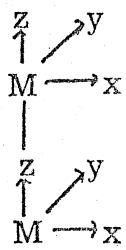

(In the HNC calculation, the nitrogen was the "metal", leading to the coordinate system depicted in the diagram). The ligand wavefunctions seem to be perfectly reasonable, and the energies are at least qualitatively correct.

For the $Rh(CNH)_4^+$ monomer, the rhodium-carbon bond length was chosen as 1.94 Å (from the crystal structure of $(Rh(CNPh)_4^+)_2$). Eigen values, symmetries, and occupancies are given in table 3, with selected eigenvectors in table 4. The calculation clearly differentiates between the occupied orbitals and the unfilled ones, as there is over a 30,000 cm^{-1} separation between the two groups. The lowest unoccupied molecular orbital is found to be the a_{2u} π^*, as expected; however, the one electron energy level diagram of $xy > xz, yz > z^2$ is not in agreement with experiment. The calculated d orbitals are found to be relatively close in energy and their order may be within the error of the calculation, however similar calculations of $Pt(CN)_4^=$ also yield incorrect orderings of this type. In fact, the orbitals are so close in energy that interelectronic repulsions might dominate the term energies, and the calculated values may actually be the correct one-electron levels. Thus, it seems that this error is a function of the method itself, and not of the particular molecule under study. In any case, the essential features of the calculations still come through, as it predicts a low-lying a_{2u} π^* orbital and a filled a_{1g} dz^2 level available for MLCT transitions.

The same calculations were carried out with identical geometries for four other metals, and the energy level diagrams are shown in tables 5 through 8. There are no major differences between any of the metals regarding the wavefunctions, with all metals retaining the

Table 1

Ligand Energies and Wavefunctions

Designation	Calculated Energy	Ab Initio Energy[3]
σ_1	-163.953	-192.70
σ_2	-104.89	-108.64
π_1	-131.58	-112.60
π_2	-44.186	- 44.026

Designation	Coefficient				
	Ns	Npz	Cs	Cpz	Hs
σ_1	.16222	-.53638	-.44657	.12086	.35988
σ_2	.09153	.28327	-.45679	.79605	-.25475
	Npx	Cpx			
π_1	.69259	.51365			
π_2	-.81833	.94101			

Table 2

Symmetry designations for all monomeric fragments.

Secular equation number	D_{4h} symmetry
1	a_{1g}
2	a_{2g}
3	a_{2u}
4	b_{1g}
5	b_{2g}
6	b_{2u}
7	e_g
8	e_u

Table 3

ENERGIES	SECULAR EQUATION	DEGENERACY	OCCUPANCY	
-199.13865	1	1	2	
-196.44786	4	1	2	
-194.49254	8	2	4	
-123.79060	4	1	2	
-120.23940	8	2	4	
-116.79980	5	1	2	
-114.96775	7	2	4	
-113.72174	3	1	2	
-112.99492	2	1	2	
-112.66602	6	1	2	
-110.53828	1	1	2	
-102.17203	8	2	4	
-86.57249	1	1	2	z^2
-84.85541	7	2	4	xz, yz
-81.61536	5	1	2	xy
-47.85485	3	1	0	π^*
-43.75497	6	1	0	
-41.53740	2	1	0	
-40.19603	7	2	0	
-40.14525	8	2	0	
-37.49693	5	1	0	
-24.22599	4	1	0	
-5.18469	3	1	0	
187.58637	8	2	0	
199.83476	1	1	0	

Energy level diagram for the $Rh(HNC)_4^+$ fragment.

Table 4

Selected Eigenvectors for the $Rh(CNH)_4$ fragment

Energy	Dz^2	s	σ_1	σ_2
-86.573	.9648	.2329	.0305	-.1120
	xy	π_1	π_2	
-81.615	.9066	.4739	.1507	
	xz	π_1	π_2	
-84.855	.9299	-.3606	.1528	
	pz	π_1	π_2	
-47.854	.3479	-.2176	.8213	

Table 5

EIGENVALUE	SECULAR EQUATION	DEGENERACY	OCCUPANCY	
-199.94320	1	1	2	
-194.73616	3	2	4	
-167.82181	4	1	2	
-120.58532	8	2	4	
-119.49822	4	1	2	
-115.44015	5	1	2	
-115.23506	3	1	2	
-114.93252	7	2	4	
-112.99492	2	1	2	
-112.66403	6	1	2	
-109.16935	1	1	2	
-102.50582	8	2	4	
-86.69039	1	1	2	z^2
-84.61495	7	2	4	xz, yz
-83.49512	5	1	2	xy
-46.00669	3	1	0	π^*
-45.88938	4	1	0	
-43.75495	6	1	0	
-41.53740	2	1	0	
-40.19611	7	2	0	
-40.04654	8	2	0	
-39.68340	5	1	0	
4.28957	3	1	0	
189.77748	8	2	0	
212.66925	1	1	0	

Energy level diagram for the $Co(CNH)_4^+$ fragment.

Table 6

[illegible]	SECULAR EQUATION	DEGENERACY	OCCUPANCY
-199.23935	1	1	2
-197.08157	3	1	2
-194.58281	8	2	4
-126.79413	4	1	2
-120.29602	8	2	4
-118.53898	5	1	2
-115.22211	7	2	4
-113.69705	3	1	2
-112.99492	2	1	2
-112.66603	6	1	2
-111.20298	1	1	2
-102.27078	8	2	4
-89.12281	1	1	2
-86.45337	7	2	4
-80.80882	5	1	2
-48.05609	3	1	0
-43.75495	6	1	0
-41.53740	2	1	0
-40.19335	7	2	0
-40.12753	8	2	0
-35.00496	5	1	0
-7.92705	4	1	0
-7.27193	3	1	0
187.92801	8	2	0
209.42001	1	1	0

Energy level diagram for $Ir(CNH)_4^+$ fragment.

Table 7

EIGENVALUE	SECULAR EQUATION	DEGENERACY	OCCUPANCY	
-195.[illegible]	1	1	2	
-195.29470	4	1	2	
-193.29234	8	2	4	
-119.43155	8	2	4	
-114.85050	4	1	2	
-114.36499	5	1	2	
-113.30268	7	2	4	
-113.06820	3	1	2	
-112.99492	2	1	2	
-112.66603	6	1	2	
-106.94551	1	1	2	
-100.94450	8	2	4	
-63.62059	7	2	4	xz, yz
-63.17480	1	1	2	z^2
-61.26361	5	1	2	xy
-45.05997	3	1	0	π^*
-43.75495	6	1	0	
-41.53740	2	1	0	
-40.55518	8	2	0	
-39.67727	7	2	0	
-36.48513	5	1	0	
-4.87208	4	1	0	
2.52066	3	1	0	
180.18510	8	2	0	
190.50576	1	1	0	

Energy level diagram for the $Ru(CNH)_4$ fragment.

Table 8

EIGENVALUE	SECULAR EQUATION	DEGENERACY	OCCUPANCY	
-201.45354	1	1	2	
-196.89847	4	1	2	
-194.88976	8	2	4	
-135.13623	4	1	2	
-123.42113	5	1	2	
-120.83131	8	2	4	
-120.51402	7	2	4	
-116.75933	1	1	2	
-114.09573	3	1	2	
-112.99492	2	1	2	
-112.66603	6	1	2	
-107.76237	1	1	2	z^2
-103.07235	7	2	4	
-102.65955	8	2	4	
-99.04994	5	1	2	xz, yz
-49.60918	3	1	0	π^*
-43.75495	6	1	0	
-42.52623	4	1	0	
-41.53740	2	1	0	
-41.18783	7	2	0	
-39.96471	8	2	0	
-38.73497	5	1	0	
-8.66297	3	1	0	
191.20377	8	2	0	
204.26787	1	1	0	

Energy level diagram for the $Pd(CNH)_4^{2+}$ fragment.

same essential bonding scheme. The charge on the metal varies in the expected fashion, becoming greater as one moves either down a period or across a row in the isoelectronic series (table 9). The Rh and Ir charges are almost identical because the VSIE's were the same(both were Co VSIE's with 10,000 cm^{-1} subtracted from the C parameters), and only the metal ligand overlaps were different for the two cases.

Relevant metal-metal overlaps for all five metals are given in tables 10through 15 . The only exceptional data is the Co $p\pi$-$p\pi$ overlap being greater than the corresponding $p\sigma$ overlap; this has been found previously to be true for Mn-Mn by Levenson[6] and occurs because of σ overlap cancelling due to the diffuseness of the 4p orbital (in fact, as the bond distance is lengthened, the $p\sigma$-$p\sigma$ overlap grows larger while the $p\pi$-$p\pi$ decreases, and eventually at about 4.3 Å the expected $\sigma > \pi$ order is restored). It should be noted that the carbon $p\sigma$ overlap with the corresponding orbital on the other monomer is very large, as is the $Np\sigma$-$p\sigma$, and these lead to a very large splitting in the energies of both the π and π^* orbitals.

A full calculation of the $(Rh(CNH)_4^+)_2$ dimer was carried out using the appropriate overlap integrals, and results are shown in table 17., with selected eigenvectors in table 18. Again, there is a clear distinction between the occupied and unoccupied orbitals, however, the energy difference has decreased by about 4000 cm^{-1}. The LUMO is , as expected, the a_{1g} bonding combination of the two a_{2u} π^* type orbitals in the fragments. Furthermore, note that although the incorrect ordering of the d levels is still maintained, <u>both</u> of the dz^2 type orbitals, the "bonding" a_{1g} and the "antibonding" a_{2u} are

Table 9

Calculated metal charge for $M(CNH)_4$ fragments

Metal	Charge
Co	0.2100
Rh	0.3168
Ir	0.3180
Ru	0.2125
Pd	0.4225

Table 10

Index for type of metal-metal overlap designation

Index	Type of overlap
1	$d\sigma$-$d\sigma$
2	$d\pi$-$d\pi$
3	$d\delta$-$d\delta$
4	$s\sigma$-$s\sigma$
5	$p\sigma$-$p\sigma$
6	$d\sigma$-$s\sigma$
7	$d\sigma$-$p\sigma$
8	$p\sigma$-$s\sigma$
9	$p\pi$-$d\pi$
10	$p\pi$ - $p\pi$

Table 11

Co-Co Overlaps

Type of Overlap	3.00 Å	3.264 Å
1	0.1826	0.0108
2	0.0083	0.0043
3	0.0011	0.0005
4	0.2968	0.2387
5	0.1086	0.2005
6	0.0417	0.0335
7	0.0076	0.0141
8	0.5775	0.5432
9	0.0312	0.0272
10	0.5413	0.4850

Table 12

Rh-Rh Overlaps

Type of Overlap	3.00 Å	3.264 Å
1	0.0369	0.0182
2	0.0138	0.0071
3	0.0017	0.0008
4	0.1578	0.1117
5	0.2988	0.2284
6	0.0556	0.0385
7	0.0859	0.0607
8	0.2187	0.1607
9	0.0306	0.0179
10	0.0737	0.0465

Table 13

Er-Ir Overlaps

Type of Overlap	3.00 Å	3.264 Å
1	0.0453	0.0287
2	0.0223	0.0120
3	0.0023	0.0014
4	0.1451	0.0999
5	0.2829	0.2074
6	0.0686	0.0474
7	0.1039	0.0729
8	0.2024	0.1439
9	0.0359	0.0207
10	0.0620	0.0373

Table 14

Ru-Ru Overlaps

Type of Overlap	3.00 Å	3.264 Å
1	0.0405	0.0253
2	0.0197	0.0106
3	0.0026	0.0012
4	0.1738	0.1261
5	0.3204	0.2517
6	0.0656	0.0472
7	0.1001	0.0736
8	0.2377	0.1792
9	0.0386	0.0234
10	0.0789	0.0504

Table 15

Pd-Pd Overlaps

Type of Overlap	3.00 Å	3.264 Å
1	0.0197	0.0105
2	0.0076	0.0035
3	0.0008	0.0003
4	0.1429	0.0988
5	0.2780	0.2069
6	0.0436	0.0286
7	0.0689	0.0461
8	0.2007	0.1439
9	0.0222	0.0125
10	0.0691	0.0431

Table 16

Symmetry designations for all dimer calculations

Secular Equation	Symmetry in D_{4h}
1	a_{1g}
2	a_{2u}
3	a_{2g}, a_{1u}
4	b_{2g}, b_{1u}
5	b_{1g}
6	b_{2u}
7	e_u
8	e_g

Two pairs of matrices involving δ-type overlaps were left degenerate, as mixing between them is very small.

Table 17

EIGENVALUE	SECULAR EQUATION	DEGENERACY	OCCUPANCY	
-200.76125	1	1	2	
-197.80779	2	1	2	
-196.34918	6	1	2	
-196.34904	5	1	2	
-194.60658	7	2	4	
-194.37364	8	2	4	
-123.79094	5	1	2	
-123.79088	6	1	2	
-120.45117	7	2	4	
-120.11775	8	2	4	
-119.48047	7	2	4	
-119.02527	1	1	2	
-117.36903	5	1	2	
-116.80019	4	2	4	
-112.99495	3	2	0	
-112.42776	1	1	0	
-110.29619	8	2	0	
-108.70653	2	1	0	
-108.01570	2	1	0	
-107.52109	6	1	0	
-102.17404	7	2	0	
-101.82346	8	2	0	
-88.25764	1	1	0	z^2 a_{1g}
-87.04028	2	1	0	a_{2u}
-85.86385	7	2	0	
-83.47412	8	2	0	
-81.61578	4	2	0	
-53.52121	1	1	0	π^* a_{1g}
-47.99519	5	1	0	
-44.04222	7	2	0	
-42.31647	7	2	0	
-42.31041	8	2	0	
-41.53740	3	2	0	
-40.41574	2	1	0	π^* a_{2u}
-38.49423	6	1	0	
-37.49695	4	2	0	
-35.32039	8	2	0	
-24.22623	5	1	0	
-24.22623	6	1	0	
-7.12947	1	1	0	
-1.34774	2	1	0	
199.14525	2	1	0	
210.74042	8	2	0	
213.59444	7	2	0	
226.36485	1	1	0	

Energy level diagram for the $(Rh(CNH)_4)_2^{2+}$ dimer at 3.264 Å. Occupancy numbers are incorrect, and filled levels are separated by the dashed line.

Table 18

Selected Eigenvalues for the $(Rh(CNH)_4)_2^{2+}$ dimer

Energy	$dz_1^2+dz_2^2$	$\sigma_1+\sigma_2$	$\sigma_2^*+\sigma_1^*$	$\pi_1+\pi_2$	$\pi_2^*+\pi_1^*$
-88.257	.9627	.2244	-.1430	.0937	.0575
-53.521	.0585	-.0103	.3831	-.2437	.7930
	$dz_1^2-dz_2^2$	$\sigma_1-\sigma_2$	$\sigma_1^*-\sigma_2^*$	$\pi_1-\pi_2$	$\pi_1^*-\pi_2^*$
-87.040	.9717	.2673	-.1327	.0752	.0278
-40.419	.0237	-.0082	.2520	-.1654	.8818

lower in energy than the monomer dz^2 orbital. This is not the case for the xz, yz orbitals, as they have split symmetrically and yielded no net bonding. Thus, the calculation conclusively shows that irrespective of the relative order of the d levels, the bonding in the $Rh_2(CNH)_8^{2+}$ dimer results from the stabilization of the filled dz^2 levels by the unoccupied π^* levels. This is in complete agreement with the molecular orbital formulation presented earlier. Furthermore, though the absolute value of the $z^2 \longrightarrow \pi^*$ transition is very far off from experiment in both the monomer and dimer, the decrease in energy between the two cases is predicted to be about 5000 cm^{-1}, while the experimental value for $Rh(CNEt)_4^+ \rightarrow Rh_2(CNEt)_8^{2+}$ is 7000 cm^{-1}.

An interesting point in this scheme is that the cause of the dz^2 stabilization is the large overlap of the carbon and nitrogen $p\sigma$ orbitals on opposite monomers. As the ligand configuration changes from eclipsed to staggered, one would expect that much of this overlap, and therefore much of the bonding, would be lost. However, the crystal structure of $Rh(CNPh)_4^+$ indicates that the dimeric units are composed of staggered monomers. It would be extremely interesting to calculate the effects that a rotation around the Rh-Rh axis would have on the total bonding, and to compare these results with experimental values.

The above analysis was also carried out with a Rh-Rh distance of 3.00 Å (table 20), and interestingly, the calculation predicted even more bonding than at 3.264 Å. Thus, according to the EH results, there is a significant driving force for two monomeric $Rh(CNH)_4^+$ units to associate, and the equilibrium bond distance is determined by a compromise between favorable electronic interactions and steric repulsions.

Table 19

Other overlaps pertinent for dimer calculations

Type of overlap	3.00 Å	3.264 Å
$C_{p\sigma}$-$C_{p\sigma}$	0.1178	0.0896
$N_{p\sigma}$-$N_{p\sigma}$	0.0602	0.0415
$Rh_{d\sigma}$-$Br_{p\sigma}$	0.0593	-----
$Rh_{d\pi}$-$Br_{p\pi}$	0.0225	-----
$Rh_{p\sigma}$-$Br_{s\sigma}$	0.1277	-----
$Rh_{p\sigma}$-$Br_{p\sigma}$	0.2305	-----

Table 20

EIGENVALUE	SECULAR EQUATION	DEGENERACY	OCCUPANCY	
-201.58592	1	1	2	
-197.27441	2	1	2	
-196.34547	6	1	2	
-196.34504	5	1	2	
-194.67474	7	2	4	
-194.30400	8	2	4	
-123.79094	5	1	2	
-123.79094	6	1	2	
-120.89252	7	2	4	
-120.70359	1	1	2	
-120.51764	7	2	4	
-120.02269	8	2	4	
-116.77338	5	1	2	
-116.80019	4	2	4	
-112.26442	1	1	0	
-112.99495	3	2	0	
-108.37679	8	2	0	
-107.84854	2	1	0	
-105.82176	2	1	0	
-105.46562	6	1	0	
-102.27429	7	2	0	
-101.71176	8	2	0	
-89.89351	1	1	0	z^2 a_{1g}
-87.43617	2	1	0	a_{2u}
-86.97115	7	2	0	
-82.69820	8	2	0	
-81.61578	4	2	0	
-55.07452	1	1	0	π^* a_{1g}
-49.29375	5	1	0	
-45.21570	7	2	0	
-42.31982	7	2	0	
-42.31056	8	2	0	
-41.53740	3	2	0	
-37.51602	2	1	0	
-37.49695	4	2	0	
-36.33871	6	1	0	
-33.31038	8	2	0	
-24.22623	5	1	0	
-24.22623	6	1	0	
-7.55297	1	1	0	
0.66684	2	1	0	
205.34189	2	1	0	
210.06114	8	2	0	
214.60483	7	2	0	
245.88779	1	1	0	

Energy level diagram for the $(Rh(CNH)_4)_2^{2+}$ dimer at 3.00 Å. Occupancy numbers are incorrect, and filled levels are above the dashed line.

Though the dimer calculations were not carried out with the other metals, inspection of the metal-metal overlaps indicate that one would expect similar interactions in all of these molecules. In all cases, the dominating overlap is the π^*-π^* which will lead to stabilization of the dz^2 levels and supply the driving force for oligomerization. Indeed, some iridium and cobalt isocyanides are reported to exist in forms of identical compositions but different colors,[7] and these calculations imply that these differences may be accounted for by association in the solid state.

The charge of the rhodium atom in $Rh_2(CNH)_8^{2+}$ is anomalously low, 0.3168, as similar calculations with the electron rich $W(CO)_6$ assign it a charge of over 0.4. This low charge is consistent with the unusual basicity of the rhodium dimer, however it does not explain why the monomers do not protonate in strong acid. In cases such as these, it is advantageous to have a method of solving self-consistently for the charge on the metals in the dimer, instead of being forced to assume the same charge for both cases.

In order to set up the calculations for the oxidative addition adducts of $Rh_2(bridge)_4^{2+}$, the fragments of $Br\text{-}Rh(CNH)_4^{+}$ and of $H\text{-}Rh(CNH)_4^{2+}$ were calculated, and the results are displayed in tables 21 and 22 . For the bromine fragment, the unpaired electron is in the a_{1g} dz^2 level, as one would expect if a d^7-d^7 metal-metal bond would be formed upon combination with another fragment. The protonated form leads to a less straightforward analysis, as it must be mixed with the bromide fragment to model the blue protonated species of $Rh_2(bridge)_4^{2+}$ in aqueous acid.

A preliminary analysis of the $(Rh(CNH)_4Br)_2$ dimer has been

Table 21

EIGENVALUE	SECULAR EQUATION	DEGENERACY	OCCUPANCY	
-[illegible]	6	6	4	
-699.47677	4	6	4	
-696.99407	4	6	4	
-695.04668	8	4	4	
-630.39979	4	6	4	
-624.48308	8	4	4	
-620.68550	5	6	4	
-607.40739	7	4	4	
-604.59943	6	6	4	
-604.24476	3	6	4	
-604.99492	4	6	4	
-604.66004	6	6	4	
-609.30448	6	6	4	
-605.60954	8	4	4	
-604.48903	8	4	4	
-98.75844	7	4	4	
-90.43448	5	6	4	
-87.45987	6	6	4	dσ -Br pσ
-50.03744	3	6	0	π*
-43.75497	6	6	0	
-40.53740	4	6	0	
-40.63004	7	4	0	
-39.98648	8	4	0	
-37.49674	5	6	0	
-27.49024	4	6	0	
-7.30494	3	6	0	
69.30474	8	4	0	
84.73974	6	6	0	

Energy level diagram for the $Rh(CNH)_4Br^+$ fragment.

Table 22

EIGENVALUE	SECULAR EQUATION	DEGENERACY	OCCUPANCY	
-202.41980	1	1	2	
-197.23952	4	1	2	
-195.25922	8	2	4	
-133.11428	4	1	2	
-126.03239	1	1	2	
-122.09338	5	1	2	
-121.38321	8	2	4	
-119.00105	7	2	4	
-114.56092	3	1	2	
-113.74758	1	1	2	
-112.99492	2	1	2	
-112.66602	6	1	2	
-103.11507	8	2	4	
-97.89037	7	2	4	
-93.20826	5	1	2	
-57.40975	1	1	0	$d\sigma$-H σ
-51.17733	3	1	0	π^*
-43.75497	6	1	0	
-41.53740	2	1	0	
-40.08190	7	2	0	
-39.87446	8	2	0	
-37.19505	5	1	0	
-28.49211	4	1	0	
-8.06671	3	1	0	
194.02916	8	2	0	
230.58500	1	1	0	

Energy level diagram for the $Rh(CNH)_4H^{2+}$ fragment.

performed (table 23), however, in these calculations, mixing of a bromine on one fragment with the metal of the other fragment was neglected. The results indicate that the expected σ-σ^* splitting is not nearly as large as one would expect, and the σ^* orbital is still occupied in this scheme. This calculation is clearly incorrect, as it predicts a triplet ground state for the molecule, but the analogous compound of $Rh_2(bridge)_4I_2^{2+}$ has a singlet ground state (verified by EPR data). If the σ interactions that were neglected turn out to be large (as they probably will), then the destabilization of the σ^* orbital will result in a singlet ground state and also remove the electrons from this occupied σ^* level, making it available for electronic transitions. The study of the electronic structure of the oxidative addition models and protonated models are areas of great interest, and will be pursued further in the future.

Table 23

EIGENVALUE	SECULAR EQUATION	DEGENERACY	OCCUPANCY	
-221.12125	1	1	2	
-220.47615	2	1	2	
-202.95444	1	1	2	
-197.42314	2	1	2	
-196.95627	5	1	2	
-196.95598	6	1	2	
-195.28998	7	2	4	
-194.75906	8	2	4	
-190.40051	5	1	2	
-190.40051	6	1	2	
-122.55463	7	2	4	
-122.21025	1	1	2	
-121.66554	7	2	4	
-120.68834	8	2	4	
-120.18611	4	2	4	
-115.77327	5	1	2	
-117.17067	1	1	2	
-112.99495	3	2	1	
-112.42129	2	1	0	
-111.82155	8	2	0	
-110.69041	1	1	0	
-108.06479	2	1	0	
-105.98425	2	1	0	
-105.46562	6	1	0	
-105.44989	7	2	0	
-105.10851	8	2	0	
-102.95691	7	2	0	
-102.20532	8	2	0	
-95.78981	1	1	0	z^2 a_{1g}
-95.60599	7	2	0	
-91.43825	8	2	0	
-91.13667	2	1	0	z^2 a_{2u}
-90.43288	4	2	0	
-55.09613	1	1	0	π^*
-49.29375	5	1	0	
-45.25220	7	2	0	
-41.53740	3	2	0	
-40.04240	8	2	0	
-39.86734	7	2	0	
-37.61006	2	1	0	
-37.29674	4	2	0	
-36.33867	6	1	0	
-33.14986	8	2	0	
-27.49120	6	1	0	
-27.49118	5	1	0	
11.50350	1	1	0	
18.70677	2	1	0	
190.33197	8	2	0	
194.70595	7	2	0	
210.63103	2	1	0	
255.74098	1	1	0	

Energy level diagram for the $(Rh(CNH)_4Br)_2^{2+}$ dimer at 3.00 Å. Occupancy levels are incorrect, and filled levels are above line.

References

1. C. Ballhausen and H. B. Gray, Molecular Orbital Theory, W. A. Benjamin, New York, New York, 1965.

2. E. Clementi, C. C. J. Roothaan, and M. Yoshimine, Phys. Rev., 127, 1618 (1962).

3. G. M. Schwenzer, H. F. Schaefer, III, and C. F. Bender, J. Chem. Phys., 63, 569 (1975).

4. J. W. Richardson, R. R. Powell, and W. C. Nieupoort, J. Chem. Phys., 38, 796, (1963), and J. W. Richardson, W. C. Nieupoort, R. R. Powell, and W. F. Edgell, J. Chem. Phys., 36, 1057 (1962).

5. H. Basch and H. B. Gray, Theoret. Chim. Acta., 4, 367 (1966).

6. Robert A. Levenson, Ph.D. Thesis, California Institute of Technology, 1970.

7. L. Malatesta, Isocyanide Complexes of Metals, John Wiley, New York, New York, 1969.

Appendix

Summary of the Structural Analysis of $Rh_2(bridge)_4(BPh_4)_2 \cdot 2CH_3CN$

This crystal structure was performed entirely by John Thich, who has kindly consented to make the information available for use in this thesis.

The crystal and molecular structure of $Rh_2(bridge)_4(BPh_4)_2$ has been determined from single crystal three-dimensional x-ray data collected by counter methods. Data derived from the crystal used in data collection are listed in Table 1. Of a total of 10,500 reflections measured, 4745 unique reflections having $F \geq 3\sigma$ were used in the structure solution and refinement.[1] The structure was solved by the heavy atom method and refined using full-matrix least squares techniques to a conventional R factor of 0.077.[2]

The structure consists of discrete dimeric $Rh_2(bridge)_4$ units in which equivalent Rh atoms are bridged by the four ligands. The coordination geometry around the Rh is essentially square planar. An ORTEP drawing of the dimeric unit along with the atom labelling used is shown in figure 1. Bond distances, angles, and least squares plane calculations[3] for the dimeric unit are collected in table 2. The unique tetraphenylborate molecule has comparable bond distances and angles to other determinations and thus has not been elaborated upon here. An ORTEP drawing of the unit cell packing is shown in figure 2.

A slight disorder exists in the structure. The carbon atom at y=1/4 of ligand 4 appears to be partially occupying two chemically reasonable positions in the mirror plane (C431, C432). Attempts at refining population distributions were only partially successful.

Equal populations (based on analysis of electron density maps) were finally given to both positions. Positional and thermal parameters were refined for both atoms. The solvent presented more serious problems. Residual electron density at y=1/4 was fitted with a disordered CH_3CN. No positional, thermal, or occupancy parameters were refined. Neither the disordered carbon atom nor solvent molecules are shown in the two figures. Bond distances and angles for the disordered carbon atom are listed in table 2.

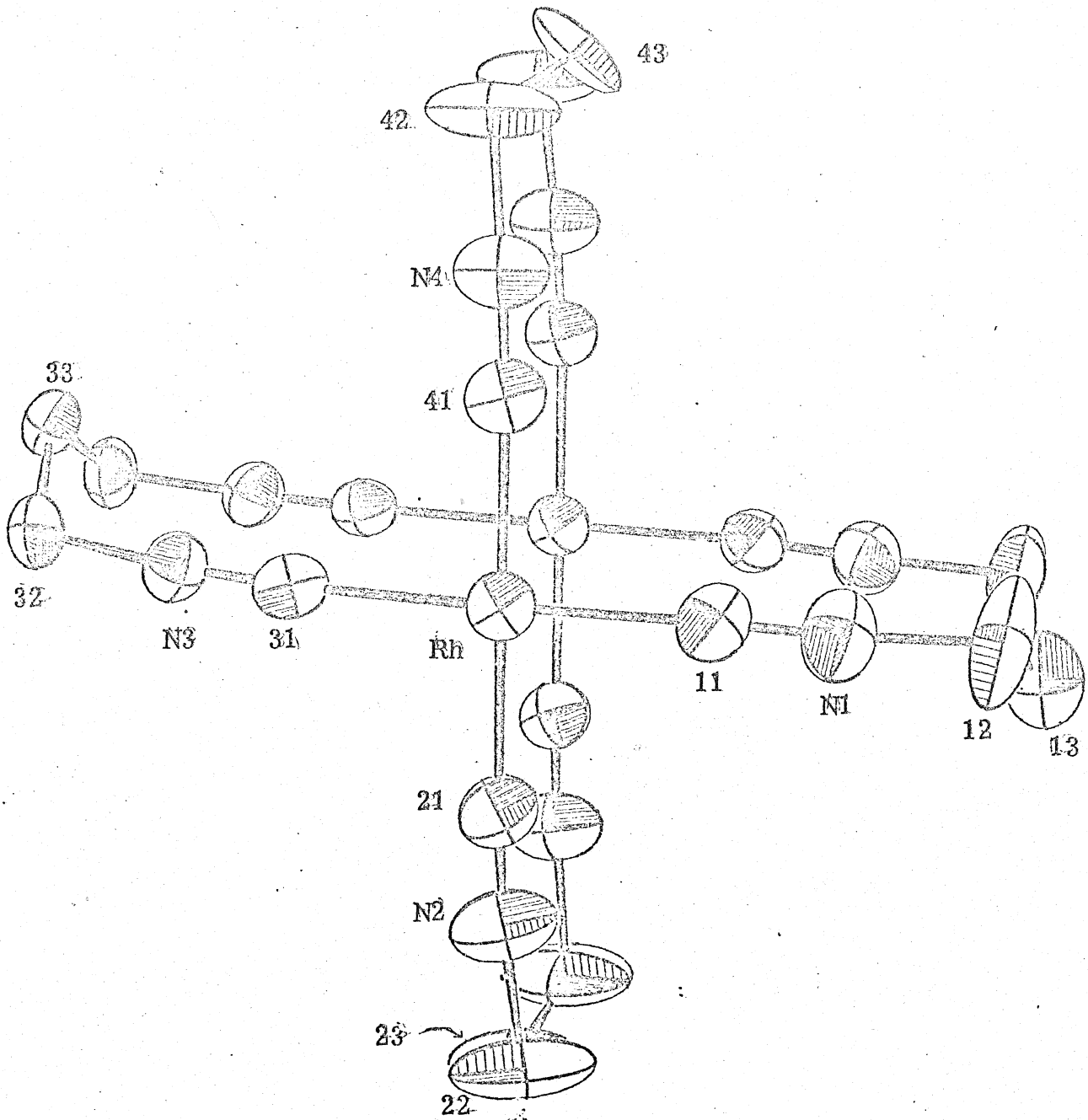

Figure 1

ORTEP drawing of $Rh_2(bridge)_4^{2+}$.

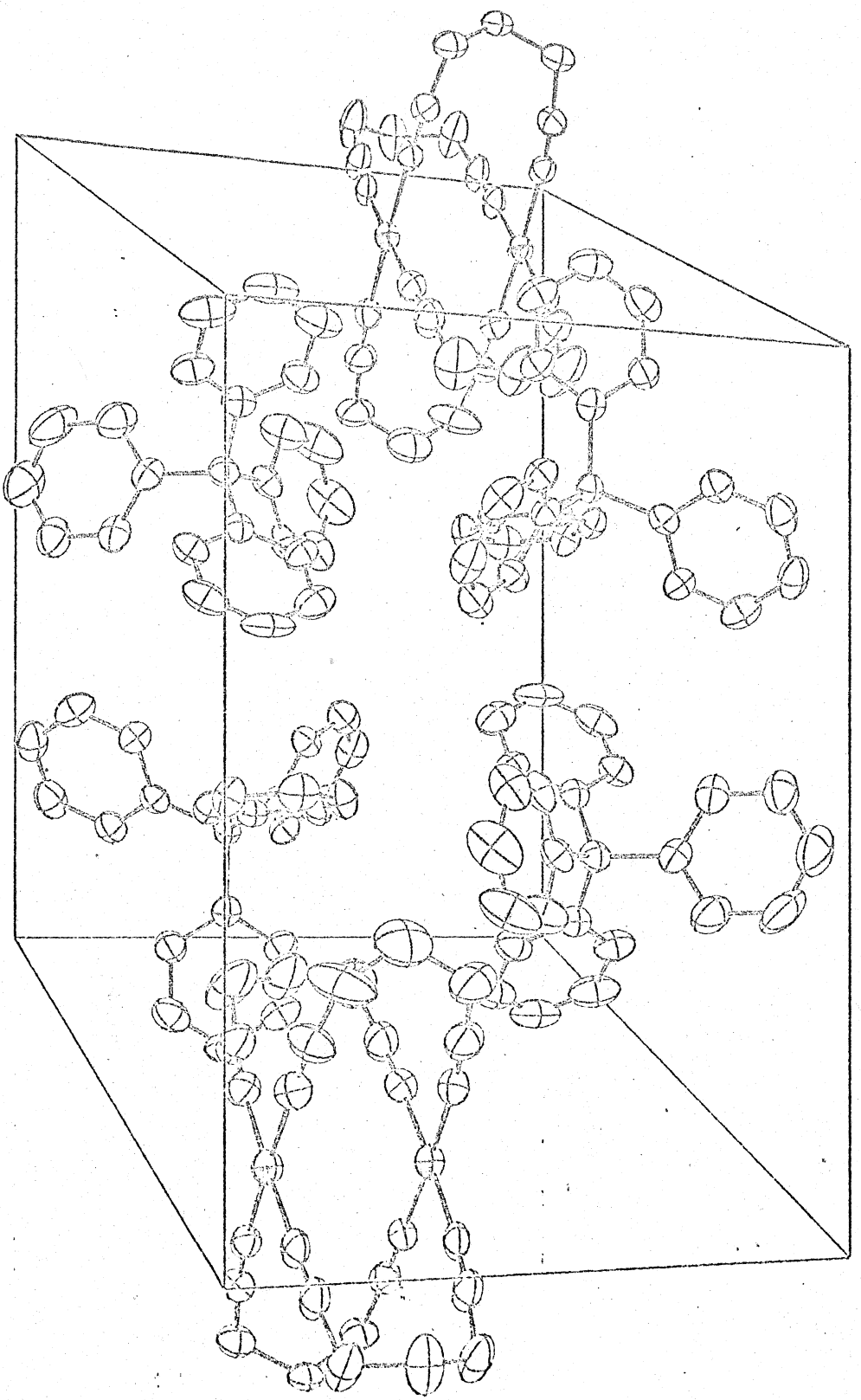

Figure 2

ORTEP drawing of unit cell packing in $Rh_2(bridge)_4(BPh_4)_2$.

Table 1

Crystal Data for $Rh_2(bridge)_4(BPh_4)_2 \cdot 2CH_3CN$

Molecular wt. =1302.8	$V = 3145\ \text{Å}^3$
Space Group=$P2_1/m$ (C_{2h}^2, No.11)	$d_{calcd} = 1.376$
$a = 17.359(6)$	$d_{obsd} = 1.306$
$b = 12.573(4)$	$\lambda = 0.71069\ \text{Å}$
$c = 15.666(8)$	$T = 22(1)\ ^\circ\text{C}$.
$\beta = 113.08(3)$	$\mu = 5.67\ \text{cm}^{-1}$

Table 2

Bond Lengths and Angles

Lengths

Rh-C11 1.966(6)	Rh-C21 1.968(6)	Rh-C31 1.983(5)
Rh-C41 1.963(5)	C11-N1 1.122(8)	N1-C12 1.432(10)
C21-N2 1.138(8)	N2-C22 1.461(10)	C31-N3 1.137(7)
N3-C32 1.446(7)	C41-N4 1.141(7)	N4-C42 1.455(9)
C12-C13 1.453(11)	C22-C23 1.356(13)	C32-C33 1.509(7)
C42-C4-3-1 1.389(14)	C42-C4-3-2 1.415(12)	
Rh-Rh' 3.264(1)		

Angles

Rh-C11-N1 176.52(57)	C11-Rh-C21 88.28(25)
C11-Rh-C31 177.21(24)	C21-Rh-C31 92.20(24)
Rh-C31-N3 175.25(51)	C11-Rh-C41 91.24(25)
Rh-C21-N2 175.05(57)	C21-Rh-C41 177.92(25)
C31-Rh-C41 88.19(24)	Rh-C41-N4 175.05(53)
C11-N1-C12 174.39(68)	N1-C12-C13 112.92(67)
C21-N2-C22 174.64(70)	N2-C22-C23 117.76(78)
C31-N3-C32 174.28(56)	N3-C32-C33 110.82(47)
C41-N4-C42 175.45(62)	N4-C42-C4-3-1 118.20(75)
N4-C42-C4-3-2 113.23(66)	

LS Plane Values

Atom	Dev(A) Sig		XP	
Rh(1)	-0.005(0)	(	-0.011	0.002 -0.005)
C11(1)	0.057(6)	(	-1.847	-0.698 0.057)
N1	0.137(5)	(	-2.910	-1.049 0.137)

Table 2 (cont'd)

Atom	Dev(a)Sig		XP	
C21(1)	0.034(6)	(-0.767	1.819	0.034)
N2(1)	0.146(6)	(-1.238	2.849	0.146)
C31(1)	0.027(6)	(1.847	0.692	0.027)
N3(1)	0.109(5)	(2.933	1.021	0.109)
C41(1)	0.026(6)	(0.729	-1.816	0.026)
N4(1)	0.119(5)	(1.217	-2.843	0.119)

RMS Deviation of fitted atoms from plane=0.023

RMS value of estimated standard deviation=0.016

Least Squares Plane is the monomeric fragment plane.

References

1. Programs incorporated in the CRYM system at the California Institute of Technology were used throughout.

2. $R_F = \frac{\Sigma \| F_o | - | F_c | |}{\Sigma | F_o |}$

3. Calculation of esd's does not take into account correlations between atoms.

CHAPTER 2

SYNTHESIS AND CHARACTERIZATION OF A MOLYBDENUM ISOCYANIDE COMPLEX: AN INORGANIC CHEMIST'S JOURNEY INTO ORGANIC CHEMISTRY

Synthesis of $Mo(2\text{-pyridyl-N=C})_6$

In 1976, Mann and Gray reported that electron transfer from a metal complex to solvent could be efficiently photo-induced with compounds of the type $M(CNAr)_6$, M=Cr, Mo, W.[1,2] Due to the wide variety of metals and side groups present in these compounds, these isocyanide complexes were found to be ideal for studying competition between photosubstitution and photoredox processes. By proper choice of the ligands and metals, it was found that ligand substitution could be eliminated, and photoreduction of solvents such as chloroform and carbon tetrachloride could proceed with very high quantum yields:

$$M(CNAr)_6 \xrightarrow[CCl_3]{h\nu} M(CNAr)_6^*$$

$$M(CNAr)_6^* \xrightarrow[CCl_3]{} M(CNAr)_6^+ + \cdot CCl_3 + Cl^-$$

Φ_{436} for $W(CNPh)_6 = 0.28$

These zero-valent complexes are relatively non-polar, and dissolve only in solvents such as benzene, dichloromethane, and dioxane. As it would be highly desirable to run this reaction in aqueous solution, yielding reduction of water to hydrogen gas, it was proposed to build an aryl isocyanide complex that would dissolve in aqueous solution. The ligand chosen was 2-pyridyl isocyanide, as it was hoped that the complex, if not water soluble, would protonate and dissolve in aqueous acid. This particular ligand had not been reported in the literature, and Ugi stated that it was too unstable to isolate;[3] however its desirability for use in a metal complex warranted another attempt at its synthesis. Along the way, much organic synthesis was attempted,

and the main value of this work was the knowledge of the methods one should use to synthesize unstable isocyanide ligands. In accordance with this view, a full description of how the ligand was prepared (as well as all the methods which did not work) will be presented below.

Due to the fact that the pyridyl functionality is reactive toward dichlorocarbene, the phase transfer method of isocyanide synthesis is of no use for these classes of compounds. The remaining strategy was then to prepare a formamide from the appropriate amine, and then dehydrate it to yield the desired isocyanide:

$$R\text{-}NH_2 \longrightarrow R\text{-}NH\text{-}CHO \xrightarrow{-H_2O} R\text{-}N{\equiv}C$$

Both 2-aminopyridine and 4-aminopyridine can be purchased from commercial sources (Aldrich) however, both the formamide and isocyanide must be synthesized.

The following syntheses are divided into two sections: attempts to make the formamides, and attempts to dehydrate it and form the isocyanide.

Synthesis of Formamides

A) The standard method[4] of neat addition of equimolar amounts of ethyl formate and amine, stirring overnight and stripping off the ethanol formed yielded no reaction with either the 2- or 4- pyridyl isomers, even with heating at 80°C. for two hours. Starting amine and ethyl formate were recovered in both cases.

B) After Knunjanz,[5] 10.0 g of 2-aminopyridine was dissolved in 100 ml of 98% formic acid, and the water was distilled off. The remaining mixture was distilled under vacuum, and the entire solution fractionated

as one mixture. This clear solution solidified upon cooling to room temperature, and the solid had a melting point of 41 °C. The infrared spectrum, NMR spectrum and melting point are all consistent with the formulation of this compound as the formic acid salt of the amine, and not the desired formamide.

C) Following Armarego,[6] 12.6 ml of anhydrous formic acid and 32.8 ml of glacial acetic acid was heated at 50 °C. for two hours. The solution was cooled to 5 °C., and while stirring, a solution of 32.8 g of 2-amino-pyridine in 150 ml of benzene was slowly added. The mixture was allowed to stir for two days at room temperature, and the benzene was pulled off. Vacuum distillation yielded two fractions, one again being the amine salt, and the other, 0.1 g, melts at 69-71 °C. (reported m.p. for 2-formamidopyridine is 71-73 °C.). Although the compound was indeed formed, it was contaminated with the amine salt, and the small yield forced other methods to be tried also.

D) Phenyl formate was prepared by the method of Yale,[7] and the 2-aminopyridine was treated with this formylating reagent as follows: the 100 g of phenyl formate solution containing about 50% phenol (by NMR integration) and 50% phenyl formate was added to 38.5 g of 2-aminopyridine at 0 °C. After stirring for ten minutes, the solution was distilled, with the low boiling fraction distilling at 45-55 °C. being excess phenyl formate-phenol, while the pale yellow residue left in the flask solidified upon cooling to room temperature and gave an NMR spectrum in $CHCl_3$ identical to that of pure 2 formamidopyridine, and as a KBr pellet, had a strong band at 1690 cm^{-1} in the infrared spectrum.

This method works quite well for excellent yields of both the 2-formamidopyridine and the 4-formamidopyridine compounds.

Synthesis of 2-isocyanopyridine

In agreement with the literature reports (actually the absence thereof), dehydration of the 2- and 4- isomers of the formamidopyridines with $POCl_3$/pyridine,[8] $POCl_3$/K -t-butoxide/t-butanol,[9] $POCl_3$/quinoline,[10] $POCl_3$/4-(3-phenylpropyl)pyridine, $POCl_3/Et_3N/CH_2Cl_2$,[11] and p-tolunesulfonyl chloride/pyridine[12] mixtures by standard methods and modified literature preparations all failed to yield any substance with the characteristic smell or $\nu(C{\equiv}N)$ at 2110 cm^{-1} of an aryl isocyanide. The following procedure was the only method found that would give any amount of the desired isocyanide.

12.2 g (0.1 moles) of 2-formamidopyridine was added to 9.7 ml of CCl_4, 11.0 ml of Et_3N, 32.2 g of PPh_3, and 100 ml of CH_2Cl_2. The entire mixture was refluxed for two hours, and was then cooled to room temperature. The crystalline solid, presumably $O{=}PPh_3$, was filtered, the CH_2Cl_2 stripped off, and the residue extracted 8 times with 25 ml portions of 30-60° petroleum ether. The ether solution was filtered and concentrated, yielding 1.2 g of a reddish-brown liquid. This liquid smelled like an isocyanide, and also possessed a very intense band as 2112 cm^{-1}, consistent with the formulation as 2-isocyanopyridine. PMR spectra also verified this structure, showing complex resonance patterns with all peaks between 8 and 10 δ. Excessive heat resulted in loss of the material; on several occasions, any attempted distillation, as well as heating excessively on a hot plate caused polymerization. Column chromatograhpy on silica gel with

2.5 : 1 CH_2Cl_2/acetone as elutant was used to purify the compound, but upon concentration of the fractions, the same reddish brown color was obtained.

Synthesis of Mo(2-pyridyl-N=C)$_6$

The desired complex was synthesized by adding 1.6 g of the 2-isocyanopyridine ligand to 0.1 g of $Mo_2(CH_3COO)_4$ in degassed methanol. After stirring for ten minutes, the solution was heated until all the yellow $Mo_2(CH_3COO)_4$ had dissolved. The solution was then cooled and yielded red crystals. The infrared and electronic absorption spectra are virtually identical with other complexes of the form $Mo(CNAr)_6$[1,13] showing a broad C≡N strecthing mode at 1960 cm^{-1} in the infrared, and bands at 440 and 493 nm in the visible spectrum.

Although insoluble in water, this complex dissolves in 12 M HCl to yield a red solution; however a thermal reaction with the acid leads to destruction of the complex in a few minutes, producing a pale yellow solution. Similar reactivity has been observed recently for other $Mo(CNAr)_6$ complexes when treated with gaseous HCl in organic solvents,[14] so the problem is not related to the pyridyl side group, rather it seems to be a property of the isocyanide functionality itself.

Although the desired Mo(2-pyridyl-N=C)$_6$ complex was not stable in aqueous acid, the most important facet of the project was the experience with methods for isocyanide synthesis, especially thermally unstable isonitriles. My general feelings on isocyanide syntheses are summarized below, as they might be of use to workers at a later date.

The phosgene method works quite well,[15] provided the lab is set up for working with large quantities of this highly poisonous gas. If one chooses to avoid phosgene, the present method of choice is the $PPh_3/Et_3N/CH_2Cl_2$ mixture,[16] which is the one used to dehydrate the 2-formamidopyridine. This mixture is widespread as a dehydrating reagent, and is a general route to isocyanides, cyanides, amides, and virtually any product of α-loss of H_2O. Also, the reaction is very clean and does not require water quenching (as the $POCl_3$, PCl_5, and other similar reagents do), but only calls for a simple extraction and removal of solvent.

The next method to be used is a specific isocyanide forming reagent: $SOCl_2$ in DMF solution.[17] This works well in most cases, however it does require a water quenching step, and for water soluble isocyanides this is somewhat of a problem. After these methods, the conventional $POCl_3$/pyridine, $Et_3N/CH_2Cl_2/POCl_3$ or other combinations will work for common side groups, as will the p-tolunesulfonyl chloride/quinoline mixture.

All of the above reagents require the formamide as a starting material. This is most conveniently prepared by adding ethyl formate to the desired amine, stirring for two hours, and removing the ethanol formed. For unreactive amines, the formic-acetic anhydride mixtures sometimes work, but phenyl formate is by far the most powerful formylating agent, and reacts with virtually every amine to yield the corresponding formamide.

For routine, everyday preparations of common alkyl or aryl isocyanides, the phase transfer method used to synthesize bridge (see part 1) is the most dependable, least expensive, and least time-

consuming of all the syntheses. It is the most suitable method for large quantities of material (1-2 moles), and it is recommended that one try this method first before resorting to any of the dehydration schemes.

References

1. Kent Mann, Ph.D. Thesis, California Institute of Technology, 1976
2. K.R. Mann, H.B. Gray, and G.S. Hammond, J. Amer. Chem. Soc., 99,306 (1977).
3. I. Ugi, Isonitrile Chemistry, Academic Press, New York, New York, 1971.
4. R.T. Morrison and R.N. Boyd, Organic Chemistry, Allyn and Bacon, Boston, Massachusetts, 1967.
5. A.E. Tschitschibabin and I.L. Knunjanz, Chem. Ber., 64,2841 (1931).
6. W.L. Armarego, J. Chem. Soc., Part 2, 2778 (1965).
7. H.L. Yale, J. Org. Chem., 36,3238 (1971).
8. W.P. Weber, G.W. Gokel, and I.K. Ugi, Angew. Chem. Internat. Ed., 11,530 (1972).
9. J. Hine and M. Hine, J. Amer. Chem. Soc., 74,5266 (1952).
10. J. Casanova, E.R. Schuster, and N.D. Werner, J. Chem. Soc, 4280 (1963).
11. W.R. Hertler and E.J. Corey, J. Org. Chem., 23,1221 (1958).
12. C.K. Ingold, J. Chem. Soc., 125, 87 (1924)
13. K.R. Mann, M. Cimolino, G.L. Geoffroy, G.S. Hammond, A.A. Orio, G. Albertini, and H.B. Gray, Inorg. Chim. Acta, 16, 97 (1976).
14. Bob Richman, personal communication.
15. I. Ugi, U. Fetzer, U. Eholzer, H. Knupfer, and K. Offermann, Angew. Chem., 77,492 (1965).
16. R. Appel, R. Kleinstuck, K.D. Ziehn, Angew. Chem. Internat. Ed., 10,132 (1971).
17. H.M. Walborsky and G.E. Niznik, J. Org. Chem., 37,187 (1972).